END
DATE
FILMED
6-80
DTIC

SC, A066547

REPORT DOCUMENTATION PAGE		READ INSTRUCTIONS BEFORE COMPLETING FORM
1. REPORT NUMBER	2. GOVT ACCESSION NO. AD-A083643	3. RECIPIENT'S CATALOG NUMBER
4. TITLE (and Subtitle) The Effect of Ion Plating and Ion Implantation on the Cyclic Response and Fatigue Crack Initiation of Metals and Alloys		5. TYPE OF REPORT & PERIOD COVERED Technical Report No. 2 1 March 1979 — 29 Feb 1980
		6. PERFORMING ORG. REPORT NUMBER
7. AUTHOR(s) S. B. Chakrabortty, S. Spooner, and E. A. Starke, Jr.		8. CONTRACT OR GRANT NUMBER(s) N00014-78-C-0270
9. PERFORMING ORGANIZATION NAME AND ADDRESS Fracture and Fatigue Research Laboratory Georgia Institute of Technology Atlanta, GA 30332		10. PROGRAM ELEMENT, PROJECT, TASK AREA & WORK UNIT NUMBERS 571
11. CONTROLLING OFFICE NAME AND ADDRESS Metallurgy Program, Material Sciences Div. Office of Naval Research 800 N. Quincy St., Arlington, VA 22217		12. REPORT DATE 1 April 1980
		13. NUMBER OF PAGES 56
14. MONITORING AGENCY NAME & ADDRESS(if different from Controlling Office)		15. SECURITY CLASS. (of this report) Unclassified
		15a. DECLASSIFICATION DOWNGRADING SCHEDULE

16. DISTRIBUTION STATEMENT (of this Report)

unlimited

DISTRIBUTION STATEMENT A
Approved for public release
Distribution Unlimited

LEVEL III

17. DISTRIBUTION STATEMENT (of the abstract entered in Block 20, if different from Report)

18. SUPPLEMENTARY NOTES

DTIC
S E
APR 28 1980
D

19. KEY WORDS (Continue on reverse side if necessary and identify by block number)

ion plating, ion implantation, fatigue

20. ABSTRACT (Continue on reverse side if necessary and identify by block number)

Fatigue crack initiation can be affected by surface phenomena and the possibility exists for improving the fatigue performance by altering the state of the surface without greatly changing bulk properties. This program was initiated on 1 March 1978, with the objective of determining the effect of ion implantation and ion plating on the cyclic stress-strain response and fatigue crack nucleation of a metal substrate. To meet this objective, we have selected surface film-substrate combinations designed to separate the various parameters, e.g., crystal structure, SFE, shear modulus, misfit, residual stress, etc., which
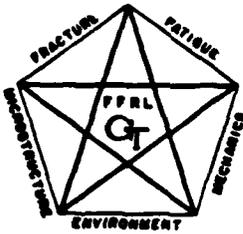
DD FORM 1473 1 JAN 73

ADA083643

DDC FILE COPY

control near surface deformation and associated crack initiation. This report summarizes our progress during the period 1 March 1979 - 29 February 1980. Three aspects of the program are discussed: (1) The effect of silver and nickel ion plating on the low and high cycle fatigue behavior of polycrystalline copper, (2) x-ray diffraction analysis of ion implanted crystals, and (3) the effect of aluminum-ion implantation on the fatigue crack initiation of poly-crystalline copper.

TECHNICAL REPORT 2
FOR THE PERIOD
1 MARCH 1979 - 29 FEBRUARY 1980

THE EFFECT OF ION PLATING AND ION IMPLANTATION
ON THE CYCLIC RESPONSE AND FATIGUE CRACK
INITIATION OF METALS AND ALLOYS

BY

S. B. CHAKRABORTTY, S. SPOONER, AND E. A. STARKE, JR.
FRACTURE AND FATIGUE RESEARCH LABORATORY

RESEARCH REPORT
CONTRACT N00014-78-C-0270

PREPARED FOR
OFFICE OF NAVAL RESEARCH
DEPARTMENT OF THE NAVY

APPROVED FOR PUBLIC RELEASE;
DISTRIBUTION UNLIMITED

PERMISSION IS GRANTED THE U.S. GOVERNMENT
TO REPRODUCE THIS REPORT IN WHOLE OR IN PART.

GEORGIA INSTITUTE OF TECHNOLOGY
ATLANTA, GEORGIA   30332

80   4 28 115

TABLE OF CONTENTS

ABSTRACT

Fatigue crack initiation can be affected by surface phenomena and the possibility exists for improving the fatigue performance by altering the state of the surface without greatly changing bulk properties. This program was initiated on 1 March 1978, with the objective of determining the effect of ion implantation and ion plating on the cyclic stress-strain response and fatigue crack nucleation of a metal substrate. To meet this objective, we have selected surface film-substrate combinations designed to separate the various parameters, e.g., crystal structure, SFE, shear modulus, misfit, residual stress, etc., which control near surface deformation and associated crack initiation. This report summarizes our progress during the period 1 March 1979 - 29 February 1980. Three aspects of the program are discussed: (1) The effect of silver and nickel ion plating on the low and high cycle fatigue behavior of polycrystalline copper, (2) x-ray diffraction analysis of ion implanted crystals, and (3) the effect of aluminum-ion implantation on the fatigue crack initiation of polycrystalline copper.

1

I. BACKGROUND

Modern design philosophies, which are greatly affected by economical and safety factors, require the use of materials having an optimum combination of properties, e.g., fabricability, strength, fracture toughness, corrosion and fatigue resistance. It is difficult to obtain alloys, either by design or through empirical development, having the required combination since the alloy chemistry and microstructure desired for certain properties may be detrimental to others. For example, aluminum alloys which show the highest static strength are inherently susceptable to stress corrosion cracking and have poor fatigue resistance. However, for most alloy systems corrosion and fatigue behavior are greatly affected by the surface condition and surface related phenomena, and may be improved (or controlled) by altering the state of the surface without adversely changing bulk properties, e.g., fracture toughness, yield strength, and ductility.

Metallic coatings have been widely used in industry for controlling corrosion and errosion. The principle of this technique is to separate the metal being protected from the unfavorable surroundings. An improvement arises from the inertness of the coating material with the environment. Many coating techniques are now available, and include hot dipping, metal spraying, electroplating, vacuum deposition, and diffusion coatings. These methods can be divided into two general groups: those which create an abrupt interface with a composition discontinuity between the coating surface and the substrate, and those which create a composition variation at the interface. Most of these coating methods produce an undesired contaminated interface which may prove detrimental when the sample is under static or dynamic loading. For example, during electroplating there may be a simultaneous reaction (e.g.,

water is often reduced to form hydrogen) which may have a considerable influence on the mechanical properties. In addition, electroplated layers can have a wide range of compressive and tensile stresses depending upon the plating parameters, and may contain networks of microcracks with varying depths and spacing. The more recent ion plating and ion implantation methods produce a clean, strongly-adherent interface between the coating material and substrate. The compositional variation at the interface can be controlled by controlling the energy of the ions.

Although it is generally agreed that fatigue cracks originate and propagate from a free surface and that the surface condition has a considerable effect on fatigue life, research on the influence of surface films on fatigue behavior has been lacking. The fatigue process may be divided into two general areas: crack initiation and crack propagation. Improvements in fatigue life can be obtained by increasing the time to crack initiation or reducing crack growth rates, or both. However, crack initiation is more affected by the surface condition than is crack propagation, and consequently the possibility exists for improving the fatigue performance by altering the state of the surface, without greatly changing bulk properties. The present ONR program is concerned with the effects of various ion-plated and ion implanted surfaces, and their microstructure, on the CSSR and fatigue crack initiation of a copper substrate. To meet the program objectives we have selected surface film-substrate combinations designed to separate the various parameters which control near surface deformation and associated crack initiation.

The influence of ion-plated surface films and/or implanted surfaces on fatigue crack initiation depends on such parameters as: crystal structure,

stacking fault energy, composition, and mechanical properties of the surface
region and the substrate; the degree of misfit and cleanliness at the interface,
the residual stresses in the film and substrate (due to radiation damage and
the accommodation dislocation network) and the adhesion of the film. The
complex interrelationships between these parameters, as well as which ones
dominate for a given system, are presently not well understood. Consequently,
the behavior of such composites is now largely unpredictable. Our effort
during the past year has been concerned with studying the effect of ion plating
on the low cycle fatigue behavior of polycrystalline copper; characterizing the
surface structure of copper single crystals implanted with aluminum and argon
ions; and determining the effect of this implantation on fatigue crack initia-
tion.

II. THE EFFECT OF SILVER AND NICKEL ION PLATING ON LOW AND HIGH CYCLE FATIGUE BEHAVIOR OF POLYCRYSTALLINE COPPER.

The results of our previous strain controlled, LCF studies [1] have shown
that silver and nickel ion plating on copper single crystals has a significant
effect on low cycle fatigue life (Figure 1). Silver plating, which has low
SFE, reduces the propensity of PSB formation in the surface region and extends
the fatigue life over that of unplated copper crystals. Nickel plating, which
has a high SFE, has the opposite effect.

This aspect of the program was undertaken to see if similar results are
possible for polycrystalline copper. In addition, stress controlled high
cycle fatigue studies were made to see if similar changes in the fatigue life
occur in the long-life regime.

Experimental

LCF and HCF specimens were machined from annealed, electrical grade,
polycrystalline copper rod obtained from Southwire Company. The specimens were
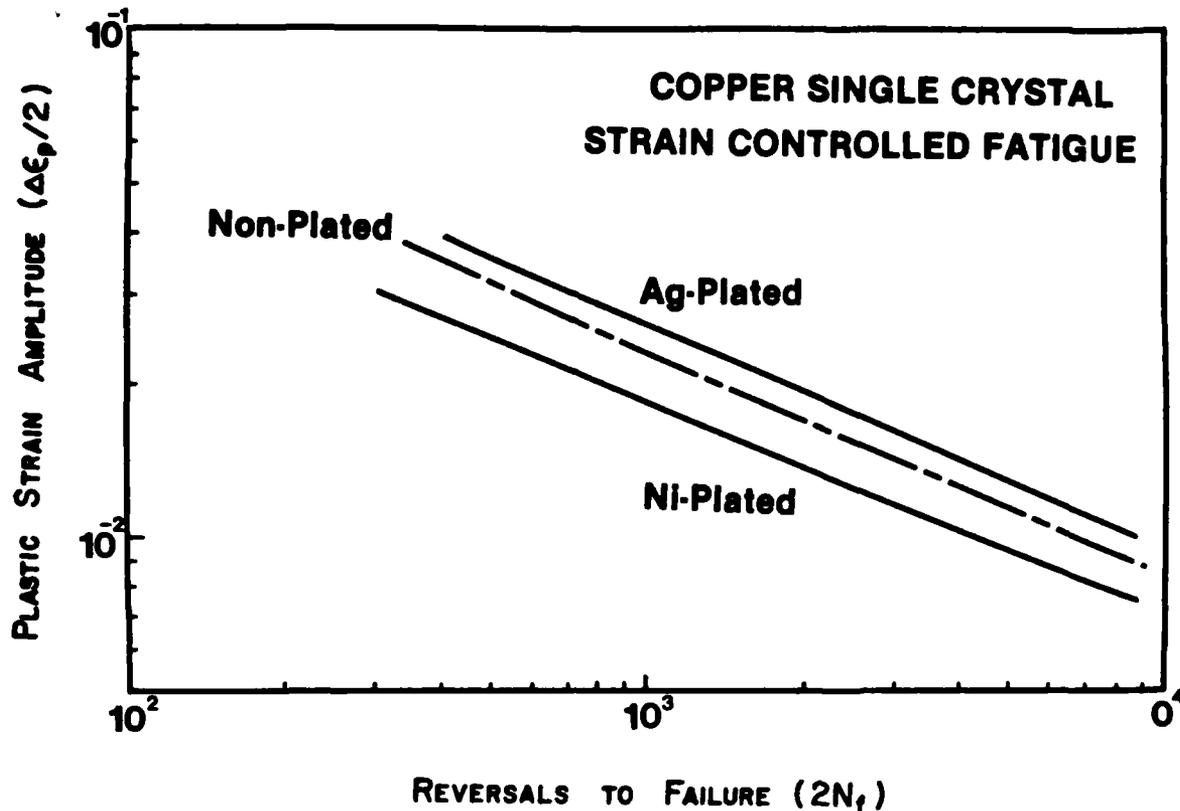
Figure 1. Strain-life curves for Ni- and Ag plated and non-plated copper
single crystals.

mechanically polished and then electropolished. Some of the specimens

sputter cleaned by argon ions at 2kv. Others were sputter cleaned and then ion

plated with either silver or nickel. A 2.5kv potential was used for obtaining

a plating thickness of 1μm. Low cycle (strain-controlled) or high cycle

(stress-controlled) fatigue tests were conducted using a servohydraulic closed-

loop testing machine. Optical and scanning electron microscopy were performed

on the fatigued samples in order to characterize the surface and near surface

defromation and crack nucleation behavior.

Results and Discussion

Several silver-plated samples have been studied and the results compared

with those obtained from non-plated samples. A limited number of nickel-

plated samples have been examined to date. However, one HCF and one LCF result

is included for comparison.

The stress-response under strain-control shows considerable cyclic hardening followed by saturation for both non-plated and plated samples, Figure 2. The cyclic stress-strain curves, Figure 3, show that the extent of hardening for the non-plated and plated samples is slightly different. Silver plating is observed to reduce the extent of hardening compared the non-plated copper, whereas nickel plating seems to have the opposite effect. The cyclic strain-life curves derived from the data, Figure 4, appear to follow the Coffin-Manson [2,3] relationship. Ag-plating improves the fatigue life and nickel plating seems to have the opposite effect. The cyclic stress-life curves, Figure 5, show an analogous effect, which is most significant at lower stresses (near the fatigue limit).

Surface slip markings on low cycle fatigue samples, Figure 6, show that silver plating leads to more homogeneous slip and reduces the propensity of persistant slip band formation. Grain boundary cracking appears to be the predominent mode of crack initiation for both the plated and nonplated materials. Surface slip markings on the high-cycle fatigue samples, Figure 7, show that slip band cracking is the predominate mode of crack initiation. at long lives. Although the density of PSB's appear to be similar for both the Ag-plated and nonplated materials the Ag-plated sample was examined after a considerably larger number of cycles. Consequently, it appears that Ag-plating reduces the propensity of PSB formation.

Deformation near the free surface has a dominate effect on the cyclic behavior of materials, especially at low strains. A surface coating of a low SFE material (e.g., Ag) modifies the surface deformation of copper towards that of silver. Under cyclic deformation slip in the surface and near surface region becomes more reversible due to a lower incidence of cross-slip. This
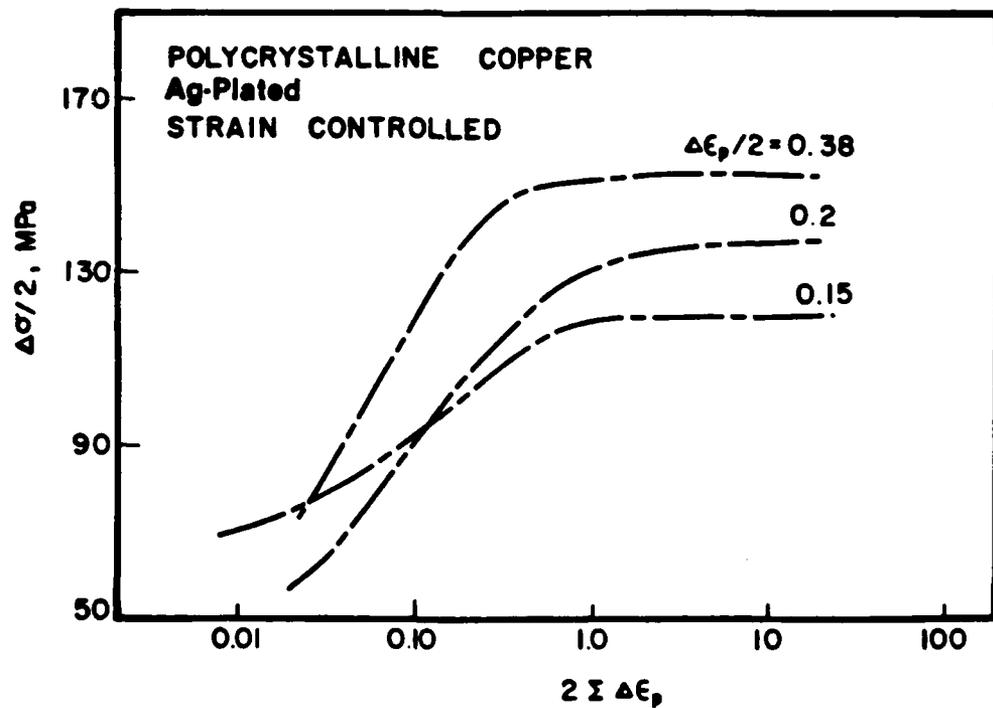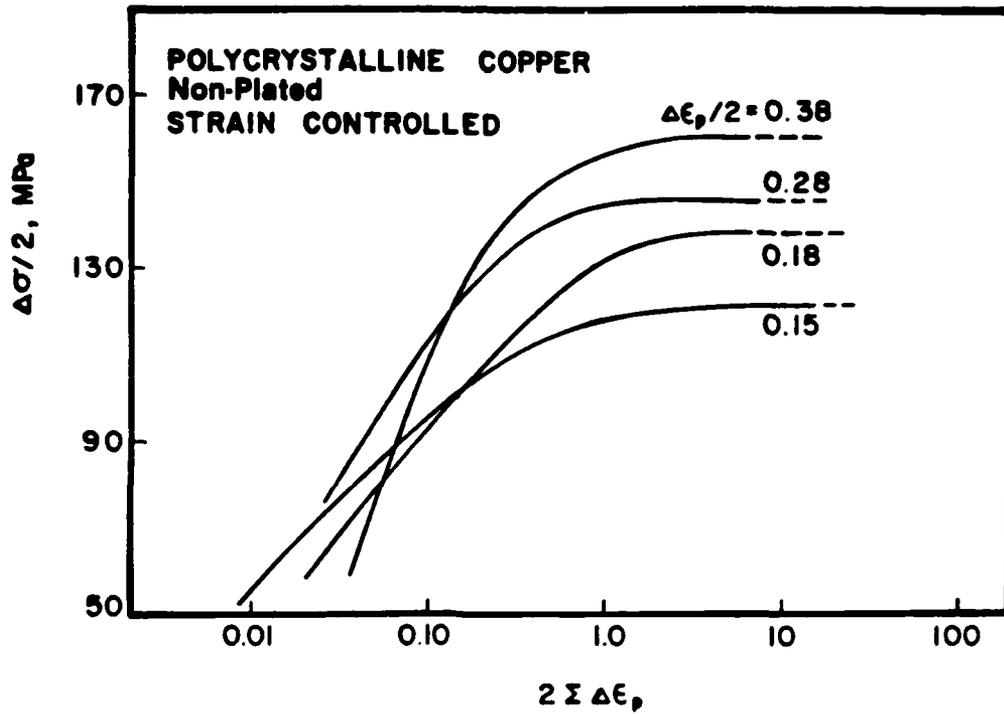
Figure 2. Cyclic stress response curves during strain controlled LCF testing.
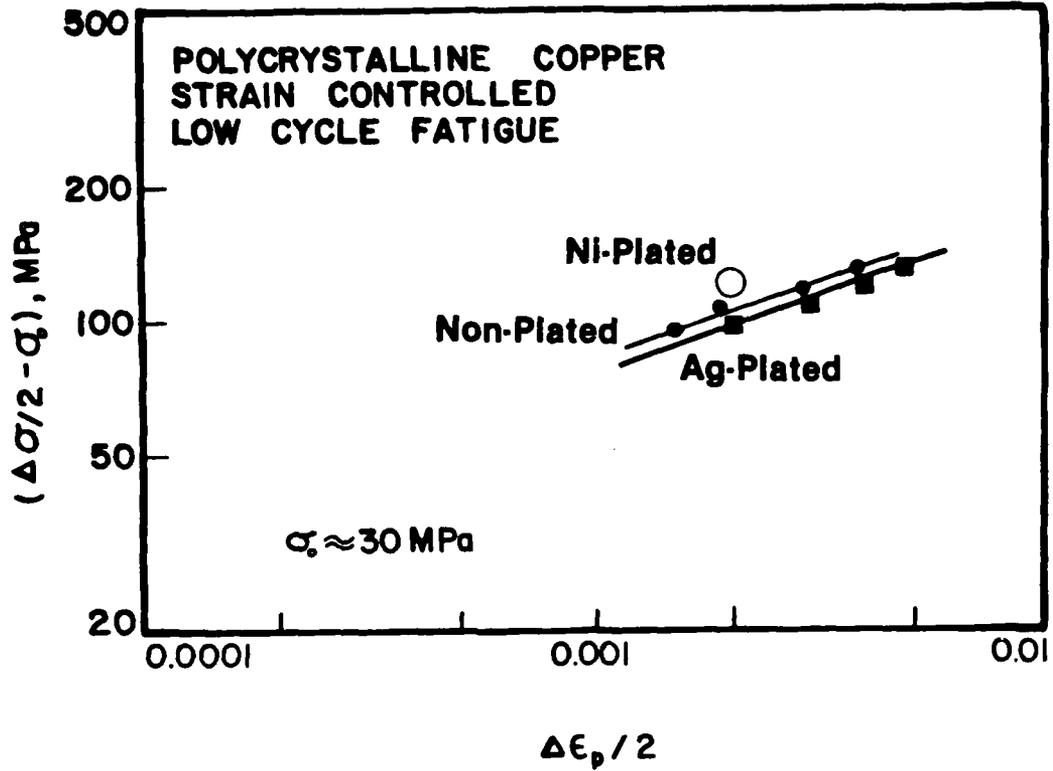
Figure 3. Cyclic stress strain curves for non-plated and Al plated
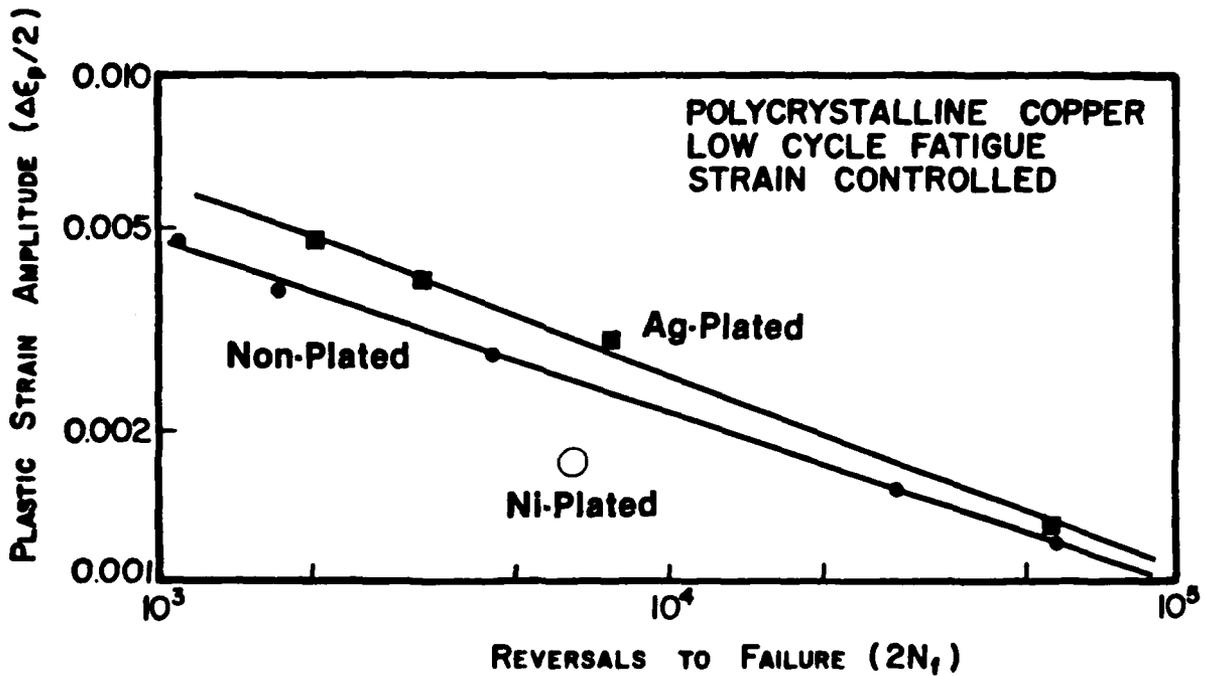polycrystalline copper.

Figure 4. Strain life curves for non-plated and Ag-plated polycrystalline
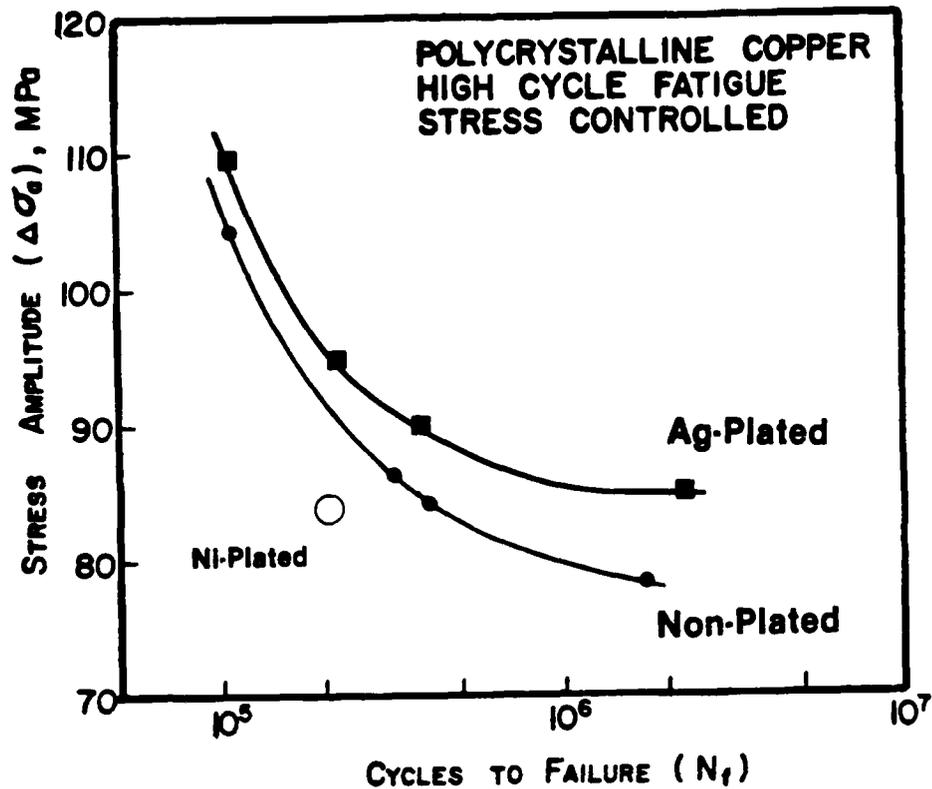copper.

Figure 5. Stress-life curves for non-plated and Ag-plated polycrystalline copper.

gives rise to more homogeneous cyclic deformation and a reduced propensity for PSB formation. Therefore, silver plating produces (1) lower cyclic hardening as a result of reduced dislocation interactions, and (2) longer fatigue life as a result of more homogeneous and reversible surface slip. These results indicate that ion plating has similar effects on the fatigue properties of both single and polycrystalline copper.

Figure 6. Scanning electron micrographs of the surface slip features of
strain-cycled polycrystalline copper samples; $\Delta\epsilon_p/2 \simeq 0.3\%$.
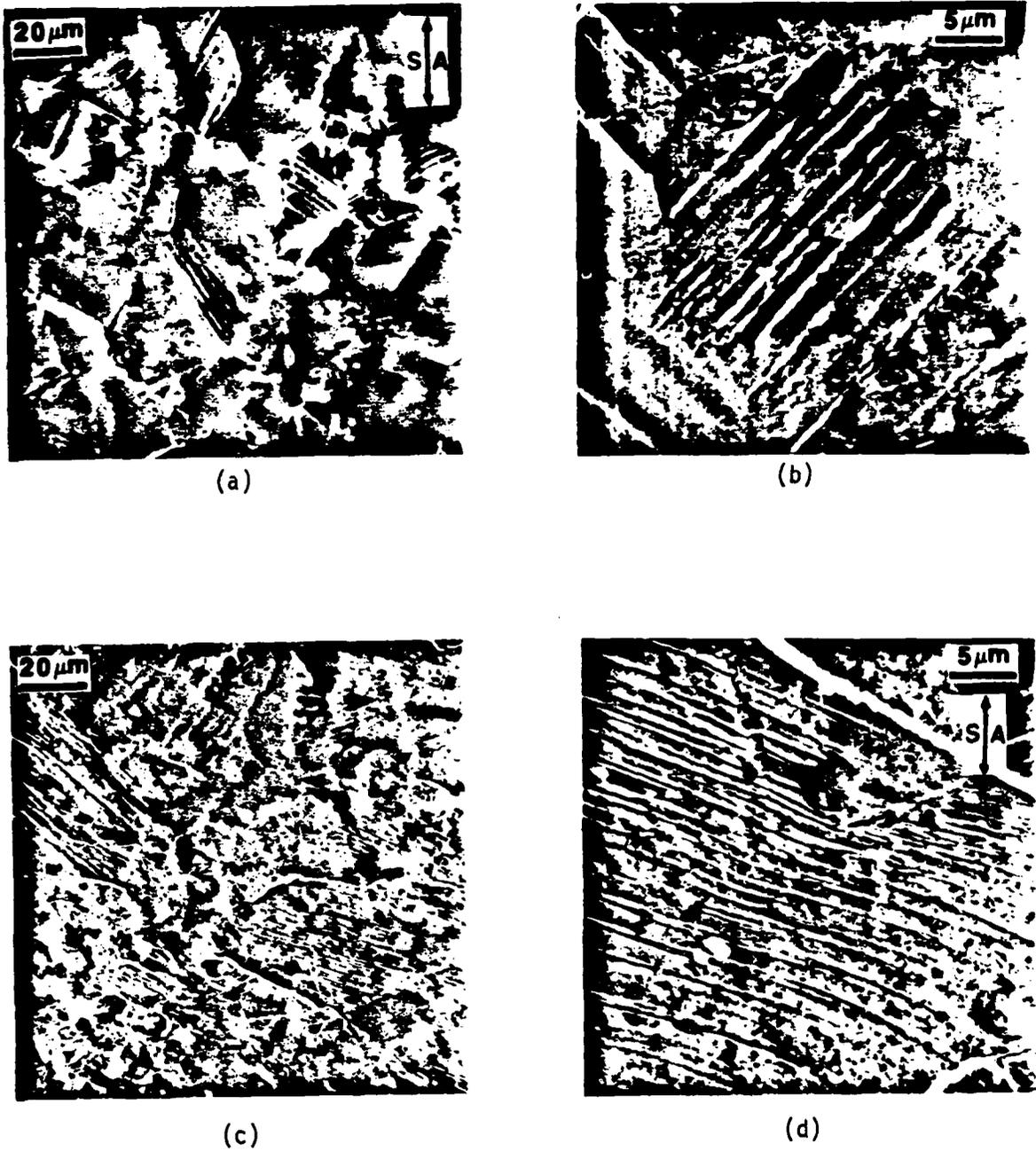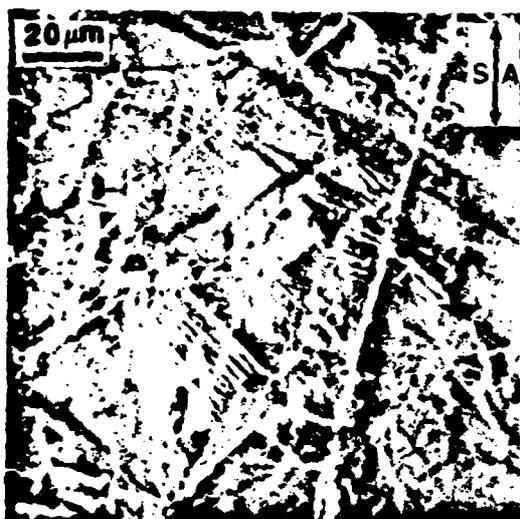(a) and (b) non-plated and sputter cleaned; (c) and (d) silver
plated.

Figure 7.   Scanning electron micrographs of the surface slip features on
             stress-cycled polycrystalline copper samples. (a) *non-plated*,
             (b) nickel-plated, (c) and (d) silver-plated.

III. X-RAY DIFFRACTION ANALYSIS OF ION IMPLANTED CRYSTALS

Some results of this aspect of our research have been prepared for publication in the proceedings of two symposia. These are included in this report as Appendices A and B. The main features of this type of analysis and our most recent results are summarized below.

The state of stress at the surface of the implanted crystal can be inferred from the lattice strain which in turn is measured by a shift in the Bragg angle. Implantation not only modifies the lattice parameter by microalloying but can severely damage the surface with the production of point defects which can also shift the lattice parameter and give a large diffuse scattering. All these effects are confined to depths much less than a micron. Non-destructive methods of implantation characterization with x-rays must employ special approaches to obtain the structural information. X-rays would not normally be useful for analysis of implantation since the sampling depth is many times the depth of the implantation affected volume. In order to avoid obscuring the scattering effects from the implanted layer, a perfect crystal substrate is used in a double-crystal diffraction arrangement. When a perfect crystal and an implanted crystal are arranged so that maximum intensity is obtained by the second reflection, the angular resolution in diffuse scattering measurements and peak shifts is measured in seconds of arc. In this way, both Bragg peak shifts and diffuse scattering from defects associated with the implanted layers can easily be measured.

Scattering from an Implanted Crystal

The two principal sources of extra scattering from an implanted single crystal are (1) the scattering from the implanted layer whose Bragg angle is changed by alloying and (2) the scattering from point defect clusters (interstital and vacancy loops). Analysis of the scattering attributed to lattice

strain due to alloying has been done in several cases where point defect scattering was not present [4]. A modification of dynamical diffraction theory can be used to calculate the reflectivity of the alloyed crystal as a function of rocking angle. To a first approximation the results of such calculations resemble the results which one might obtain using kinematic diffraction theory for a very thin crystal. In detail, however, there are interference effects which can be analyzed in terms of strain distribution to get a more detailed description of alloy distribution.

The second source of scattering dominates in the measured scattering in the implanted metals under investigation in this program. One result is that alloy distribution and strain effects are somewhat obscured. Nevertheless quantitative analysis of the damaged state of the implanted layer can be done. Scattering theory (kinematic) for scattering from dislocation loops and spherical precipitates has been worked out [5]. Diffuse scattering measured as "integral diffuse" intensity in a double-crystal experiment is given in the following formulas:

$$I^S(q_0)/I_0 = 1/(2\mu_0) \, (r_e f_h e^{-M_h})^2 (h/k)^2 \, 2\pi\tau \sum_i (c_i/V_c) (b\pi R_i^2/V_c)^2 \ln(e^{\frac{1}{2}} q_L^i/q_0)$$

for $q_0 < q_L$ and,

$$I^S(q_0)/I_0 = (1/2 \, \mu_0 V_c) \, (r e f_m e^{-M_h})^2 \, (h/k)^2 \, 2\pi\tau \, (b\pi/V_c) \, \alpha^2/2q_0^2 \, n_{PD} \quad \text{for}$$

$q_0 > q_L$ where, $I^S(q_0)$ is the average diffuse scattering intensity calculated from $(I(+q_0) + I(-q_0))/2$, $q_0 = h \cos\theta_B \, \Delta\theta$, $\Delta\theta = \theta - \theta_B$, $h = 4\pi\sin\theta_B/\lambda$, μ_0 absorption, r^e Thompson electron radius, f_h structure factor, e^{-M_h} Debye-Waller factor, $k = 2\pi/\lambda$, $2\pi\tau$ is an averaging parameter for dislocation loops, C_i/V_c is the number density of loops of radius R_i, b Burgers vector V_c unit all volume, q_L^i is α/R_i, with $\alpha = \sqrt{2}$ for the (222) reflection and n_{PD} the density of point defects. The first equation can be used to determine the loop size

distribution for the case of well determined diffuse scatterings. A simpler application uses the assumption of a single average loop radius size which can be obtained from the extrapolation of $I^S(q_0)$ vs $\ln(q_0)$ to zero where $q_0 = e^{\frac{1}{2}} q_L$ and $R^2 = \alpha/q_L$.

The second equation can be used to obtain the total point defects per volume; $I^S(q_0) q_0^2$ is proportional to n_{PD}. These formulas do not distinguish between vacancy and interstital loops since differential symmetrically averaged intensity is employed. A detailed measurement of the differential diffuse scattering rather than integral diffuse scattering is required for such distinctions to be made unambiguously.

Since the loop scattering originates in the implanted layer, the q_0 value must be adjusted for the Bragg angle shift. Since shifts are small (a few minutes) the measurement of n_{PD} which uses large q_0 values is unaffected. At small angles (q_0) asymmetry in the scattering can be used to infer Bragg angle changes. But, one must recognize that it is possible to produce asymmetry in the scattering at small angles by certain combinations of interstitial and vacancy loop scattering, each of which has opposing asymmetry.

Double Crystal Method

As mentioned earlier, the double-crystal method which uses perfect crystals has the advantage of permitting the observation of scattering at angles very close to the Bragg peak. The scattering which is measured is, in fact, diffuse scattering measured over the Ewald sphere in the vicinity of the Bragg point in reciprocal space. The range of the integration is determined by the solid angle defined by the solid angle subtended by the detector. A major portion of the measured scattering at small angles is reflected (in the dynamical theory sense) from the unimplanted subtrate and can be corrected by subtraction of scattering measured from an unimplanted surface. Fig. 8 shows

the curves for implanted and unimplanted crystal as a log intensity scale. The excess scattering although obvious on a log scale is nevertheless small (a few tenths of a percent reflectivity) over an angular range of less than a degree. The asymmetry that may be attributed to Bragg angle shift can only be measured within an angular range of ten minutes of the substrate Bragg peak.

The experimental arrangement needed for such measurements is simple. Two crystals are mounted on adjustmable goniostats. The first crystal reflects intensity from the x-ray source to the second crystal and is adjusted only once to maximize the intensity at the second crystal position. The second crystal can then be focused to reflect the incident rays into the detector (actually 85 to 90% according to theory). This is the "antiparallel" arrangement which simply means that the Bragg plane normals are perfectly parallel but are directionally opposite. As Fig. 9 shows the peak is sharp - a full width at half maximum of approximately 10 seconds. The second crystal - which is the implanted crystal - is rotated on a goniometer to give the rocking curve. Simple adjustments are sufficient to keep the detector centered on the Bragg peak intensity. Upon mounting a new sample crystal, some care must be taken to find maximum reflectivity.

Equipment

Two goniostats, motorized goniometer and conventional x-ray equipment are assembled into a double crystal apparatus. The only critical part of the apparatus is the motorized goniometer. A Huber goniometer was used with a 10-to-1 gear reducer and was driven by a SLO-SYN pulsed motor. Backlash in the goniometer gearing is but a few seconds and can be removed effectively by running rocking curves in a fixed direction. No absolute angular measurements are made since the Bragg peak from the substrate is a satisfactory internal standard. Data are collected by step-counting mode. Figure 10 shows
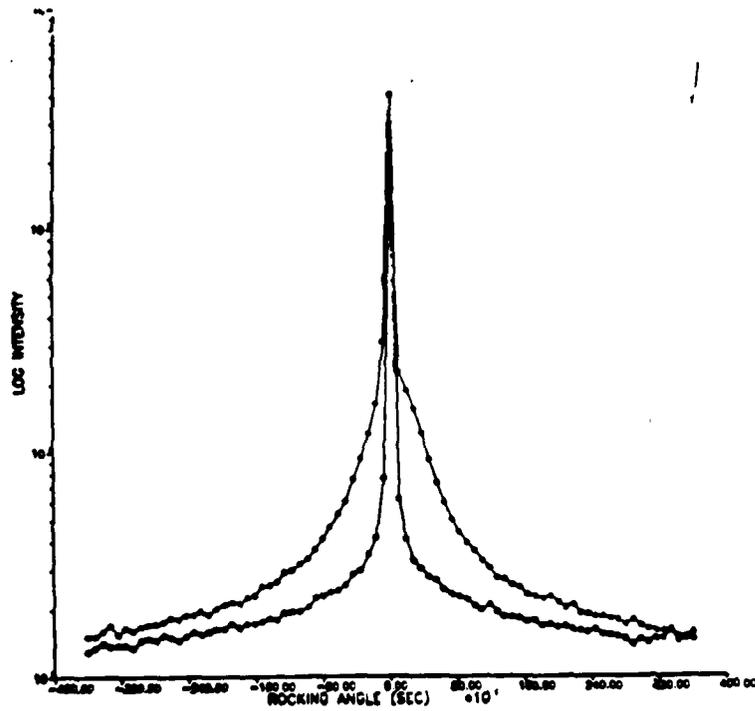
Figure 8. Log integral diffuse scattering vs. rocking angle for copper implanted with 3.4×10^{15} boron ions/cm^2.
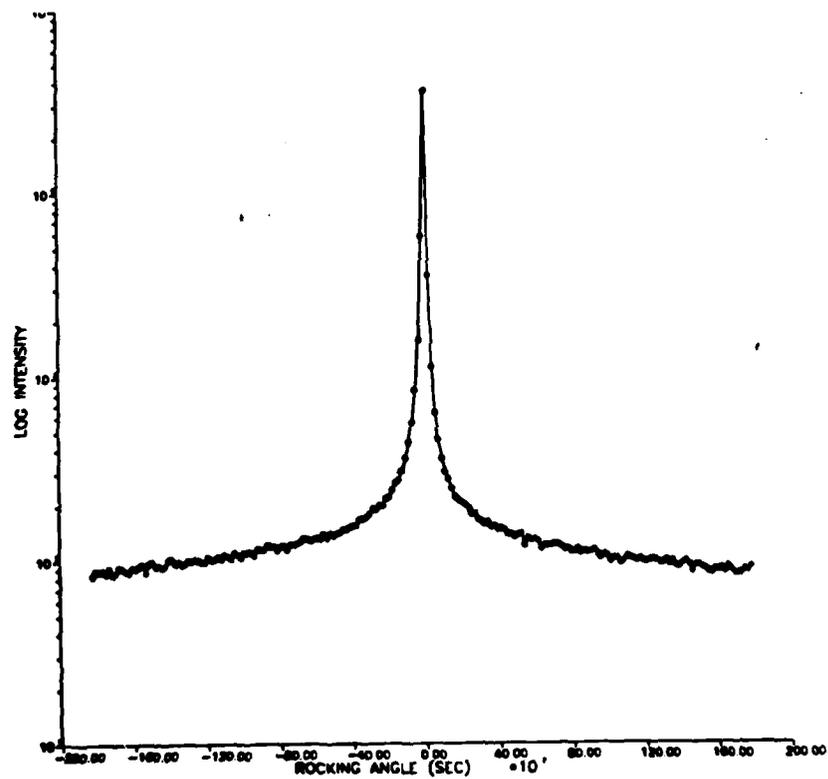

Figure 9. Sharpness of resolution is shown in the rocking curve of unimplanted copper.

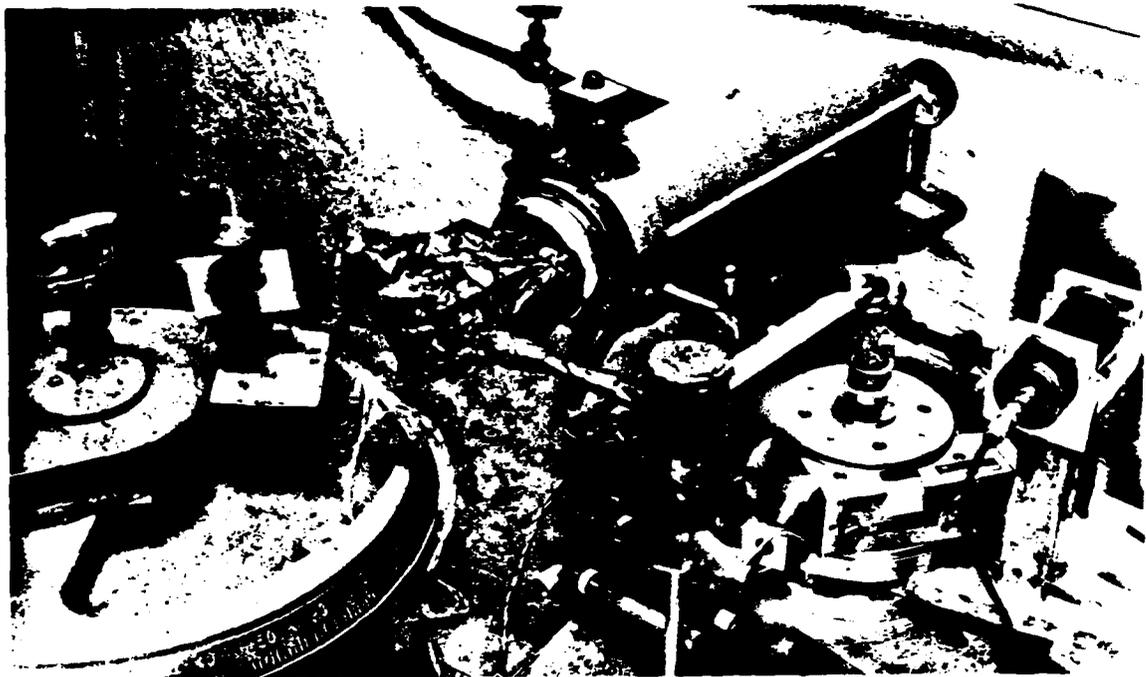a photograph of the arrangement operating with the GE XRD-7 system.

Figure 10. Layout of double crystal apparatus. The monochromating (first) crystal is enclosed in the cylindrical lead shield. A 2 mm diameter apparature near the second crystal defines the sampled area. No collimation is placed between the second crystal and the detector.

Interpretation of Boron Implantation Results

Boron implantation produces a surface alloy whose lattice parameter is less than that of copper. This can be seen in Figure 11 in which the intensity is shifted by approximately 50 arc seconds. The shift is somewhat smaller in the 1.25 dose than in the 1.00 dose and might be attributed to second order lattrice parameter changes due to a greater number of point defects. The fractional lattice parameter change calculated from this shift is -2.6×10^{-4} ($\Delta a_0 / a_0$) and with the estimated alloy composition represents a large change (10% per atomic per cent of boron). The implication of this finding is that the implanted layer will be under tensile stress by virtue of lattice parameter coherency between the implanted layer and the copper substrate (matrix).
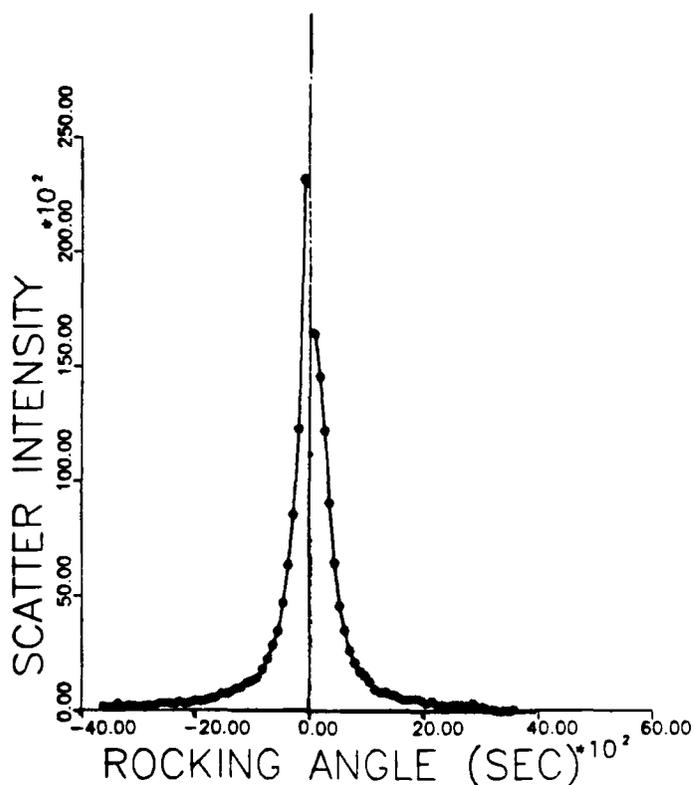
Figure 11. The angular shift toward larger angle is shown in the
excess diffuse scattering curve for copper implanted with
3.4×10^{15} boron ions/cm^2.

These data have been analyzed in terms of dislocation loop structure and
total point defect density. In Fig. 12 the symmetric excess intensity is
plotted versus ln q_0 and the intercept at zero intensity (q_0^*) is used in the
relation

$$q_0^* \ R_{loop} = e^{\frac{1}{2}\alpha}$$

with $\alpha = \sqrt{2}$ for the (222) reflection. It is found that loop radii become smaller
with dose even though the number of point defects increase with dose. Table 1
summarizes the preliminary findings for these doses. Note that the peak
boron content in the highest dose is still smaller that the quoted solubility
limit (0.34 atomic %).

TABLE I

Dose (ions/x-rayed area)	R_{loop}	Point Defects (per x-rayed area)
0.4×10^{14}	93 Å	0.4×10^{15}
1.6×10^{14}	80 Å	3.6×10^{15}
2.0×10^{14}	73 Å	3.9×10^{15}

The number of defects produced per ion is approximately 18 to 20 and is between 2 and 5% of the point defects produced as estimated by simple LSS collision theory. The density of dislocations in the implanted layer was estimated by using a 80 Å loop circumference to contain measured point defects in a layer assumed to be 3000 Å thick. The resulting dislocation density is 2.5×10^{12} cm^{-2}.
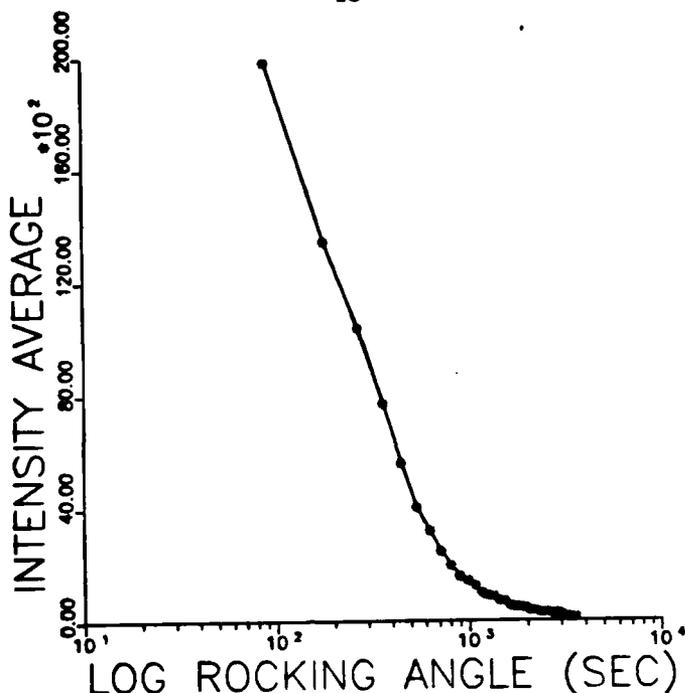
Figure 12. An average loop radius is determined from the extrapolation of intensity to zero in this plot. A llop radius of 90 A is obtained for an implantation of 3.4×10^{15} boron ions/cm^2.

IV. THE EFFECT OF ION IMPLANTATION ON THE FATIGUE CRACK INITIATION OF POLYCRYSTALLINE COPPER

Some of the results of this aspect of our research have been prepared for publication in the proceedings on the Symposium on Surface Modifications of Materials by Ion Implantations. The manuscript is included in this report as Appendix C. The main features can be summarized as follows:

Aluminum ion implantation did not seem to effect the monotonic yield stress, but did decrease the extent of work hardening in the low strain range. A similar decrease was observed in the cyclic hardening behavior. Aluminum ion implantation produced a significant improvement in fatigue life for both strain and stress controlled tests. This improvement is associated with modifications of the deformation behavior in the surface and near surface regions of the implanted copper, and its subsequent effect on fatigue crack initiation. For details, see Appendix C.

V.   PROFESSIONAL PERSONNEL

    Dr. Edgar A. Starke, Jr.
    Dr. Saghana B. Chakrabortty
    Dr. Stephen Spooner
    Dr. Keith O. Legg

VI. GRADUATE STUDENTS

    Fred Anderson
    A. Kujore
    P. Heydari-Darani

VII. PUBLICATIONS AND PRESENTATIONS

1. A. Kujore, S. B. Chakrabortty, E. A. Starke, Jr., and K.O. Legg, "The Effect of Aluminum Ion Implantation on the Fatigue Crack Initiation of Polycrystalline Copper," presented at the Materials Research Society's Symposium on Surface Modification of Materials by Ion Implantation, Cambridge, MA, November 30, 1979. To be published in the Proceedings of the Symposium.

2. Stephen Spooner and Keith O. Legg, "X-Ray Diffraction Characterizations of Aluminum Implanted Copper Crystals," presented at the Materials Research Society's Symposium on Surface Modifications of Materials by Ion Implantation, Cambridge, Ma, November 30, 1979. To be published in the Proceedings of the Symposium.

3. S. Spooner, "X-Ray Scattering Investigation of Microalloying and Defect Structure in Ion Implanted Copper," presented at the AIME Symposium on Advanced Techniques for the Characterization of Microstructures, Los Vegas, Nevada, February 24-28, 1980. To be published in the Proceedings of the Symposium.

4. P. Heydari-Darani, A. Kujore, S. B. Chakrabortty, E. A. Starke, Jr., and K. Legg, "The Effect of Ion Implantation on the Cyclic Stress Strain Response and Fatigue Crack Initiation of Copper," presented at the 109th AIME Annual Meeting, Las Vegas, Nevada, February 24-28, 1980.

5. A. Kujore, S. B. Chakrabortty, and E. A. Starke, Jr., "Low Cycle and High Cycle Fatigue Behavior of Ion Plated Polycrystalline Copper," presented at the 109th AIME Annual Meeting, Las Vegas, Nevada, February 24-28, 1980.

6. S.B. Chakrabortty, A. Kujore, and E. A. Starke, Jr., "The Effect of Ion Implantation on the Cyclic Stress-Strain Response of Polycrystalline Copper," to be presented at the International Conference on Metallurgical Coatings, April 21-25, 1980, San Diego, California.

7. S. B. Chakrabortty, K. Legg, and E. A. Starke, Jr., "The Effect of Ion Implantation on the Fatigue Properties of Polycrystalline Copper," to be presented at the Ion Beam Modification of Materials, July 14-18, 1980, Albany, N.Y.

8. E. A. Starke, Jr., S.B. Chakrabortty, and A. Kujore, "The Effect of Ion Implantation on the Fatigue Behavior of Metals and Alloys," to be presented at the Sixth Conference on the Applications of Accelerators in Research and Industry, November 3-5, 1980, Denton, Texas.

VIII. REFERENCES

1. E. Y. Chen and E. A. Starke, Jr., "Effects of Ion-Plating on the Low Cycle Fatigue Behavior of Copper Single Crystals," Materials Science and Engineering, 24 (1976) pp 209-221.

2. L. F. Coffin, Trans. AIME, 76 (1954) pp 931-950.

3. S. S. Manson, NASA, Technical Note 2933 (1954).

4. B. C. Larson, C. W. White and B. R. Appleton, "Unidirectional Contraction in Boron-Implanted Laser Annealed Silicon," Appl. Phys. Lett., 32, pp. 801-803 (1978).

APPENDIX A

X-RAY DIFFRACTION CHARACTERIZATIONS OF ALUMINUM
ION IMPLANTED COPPER CRYSTALS

By

Stephen Spooner
and
Keith O. Legg

X-RAY DIFFRACTION CHARACTERIZATION OF ALUMINUM ION

IMPLANTED COPPER CRYSTALS

Stephen Spooner
Fracture and Fatigue Research Laboratory
and
Keith O. Legg
School of Physics
Georgia Institute of Technology

X-ray diffraction from aluminum ion implanted copper is analyzed in single crystals in terms of microalloying and radiation damage effects. Sessile dislocation loop scattering dominates scattering, although asymmetry in diffuse scattering distribution can be attributed to the lattice expansion due to alloying. Annealing at 500°C for 30 minutes produces no significant change in the structure. Annealing at 600°C for 30 minutes appears to remove microalloying effects while leaving damage structure having a stability which may be effective in inhibiting fatigue crack initiation.

Introduction

Ion plating has been demonstrated to modify the fatigue crack initiation resistance in copper single crystals (1). Vapor deposition alone can change mechanical properties of copper (2) but the damage effects of ion implantation on mechanical properties remains unexplored. Studies of the structure of ion implantation damage in connection with neutron damage simulation (3) and semi-conductor device physics (4) provide a basis for such investigations. The structure of the implanted layer can be modified by choice of ion, energy, and dose. The application of implantation to the control of fatigue crack initiation must consider several fundamental questions: How do ion-type and implantation energy affect surface layer structure and structure stability? How do the various implantation structures affect fatigue crack initiation mechanisms? Which structures are helpful or detrimental to mechanical property improvements? A partial answer to some of these questions can be found in a recent presentation on the effects of platinum implantation on subsurface crack initiation in titanium. (5) In this case the treatment brings mixed benefits to the control of fracture initiation.

This x-ray diffraction investigation is part of a study on the effects of ion plating and ion implantation on fatigue crack initiation. Conventional x-ray diffraction methods depend either on measurement of peak shifts to reveal the state of residual stress (6) or peak profile analysis (e.g., the Warren-Averbach analysis) to characterize effective particle sizes and strains (7) in the material of a surface. In these investigations the property controlling imperfections are distributed over depths much greater than the penetration depth of the x-rays. However, in the case of an implanted layer, the affected material is much shallower than the x-ray penetration depth and, unless some special conditions are used, the diffraction effects from the damaged layer would be lost in the tails of the diffraction peak from the unmodified substrate sampled by the x-rays. We have adopted the use of rather perfect crystals in a double-crystal technique (8-10) used in radiation damage investigations which successfully circumvents the problems in the conventional x-ray diffraction methods. Experiments are described in which aluminum implantation effects in copper crystals including response to annealing are analyzed. It is shown that the damaged state produced by ion implantation is relatively stable against annealing and therefore may provide an effective inhibitor to surface fatigue crack initiation. The effects of aluminum implantation in poly-crystalline copper is discussed in a companion paper (11).

Experimental

Implantation of copper with aluminum ions was selected for this study because of high solubility of aluminum in copper, because of an appreciable lattice parameter change upon alloying aluminum with copper, and because the aluminum ions penetrate relatively far into the substrate at the implantation energies available to us. Thus, an alloy layer of favorable thickness will be produced which has a relatively simple microalloy structure containing ion damage effects.

Highly perfect crystals were selected for x-ray studies in order that pre-existing dislocations would not interfere with ion-implantation effects. Bulk copper crystals were provided by F. W. Young of Oak Ridge National Laboratory. These crystals were grown by Bridgeman technique and then annealed for two weeks at a few degrees below the melting point. The crystals were radiation hardened with neutrons before final cutting to orientation. Chemical cutting techniques were used to shape the crystal.

24

The dislocation densities measured after final sample preparation, but prior to ion implanation, was less than 10^3 cm^{-2}.

Two crystals were prepared with 111 faces. Each was mounted in the ion accelerator with the (111) normal 6° from the ion beam direction. An Accelerators, Inc. Ion Implanter which can be run up to 200 Kev was used to implant the crystals at 25°C. Although the temperature rise was not measured, the crystals, which have a volume of approximately 2 cc, were considered to be a sufficient heat sink allowing less than a degree temperature rise during implantation. The implantations were made in three doses each varying in energy and duration for the purpose of producing a level aluminum distribution. The dose calculations were made on the basis of the LSS model (11) of ion penetration and the dose rates were as follows: 19.7X10^{13} ions cm^{-2} sec^{-1} at 200 Kev, 9.9X10^{12} ions cm^{-2} at 100 Kev and 2.4X10" ions cm^{-2} sec^{-1} at 50 Kev. The accumulated ion doses were 2X10^{16} ions cm^{-2}, 4X10^{15} ions cm^{-2} and 5.5X10^{15} ions cm^{-2} respectively. The results of Keinonen et al. (12) are used to correct the simple LSS predictions for ion ranges giving an Al concentration of 1.8 atomic per cent over a depth of 1200 Å. Estimates of the damage profile relative to the ion profile were made using the calculations of Winterbon (13,14). The estimated profiles are shown in Figure 1.

In the double-crystal diffraction method two crystals of nearly identical d-spacing are set in the anti-parallel reflection position that eliminates wavelength dispersion. Experiments were done at the Solid State Division of Oak Ridge National Laboratory. Copper radiation was reflected first from the 333 planes of a perfect Si crystal. The implanted copper crystal was set for the 222 reflection. The two d-spacings are closely matched. A 3 mm diameter area was implanted on the (111) Cu crystal surface so that both on implanted and unimplanted region could be investigated in the same crystal surface. The copper crystal is rotated through the diffraction peak position and the intensities are normalized to the incident beam which was measured by the detector through a calibrated filter. The scattering vector diagram in Figure 2 shows the arrangement where an open detector with no intervening collimation intercepts scattering from over an area of the Ewald scattering sphere. Scattering measurements were made on the implanted and unimplanted surface of each crystal. With the intention of exploring
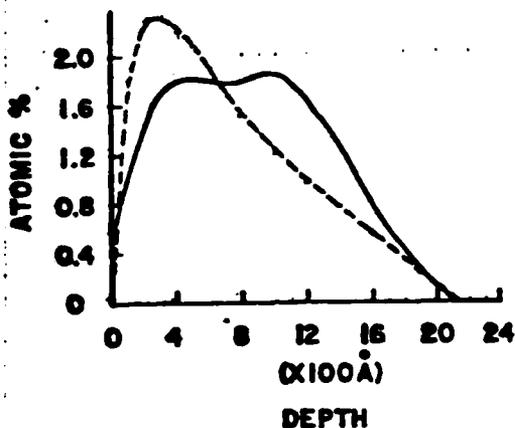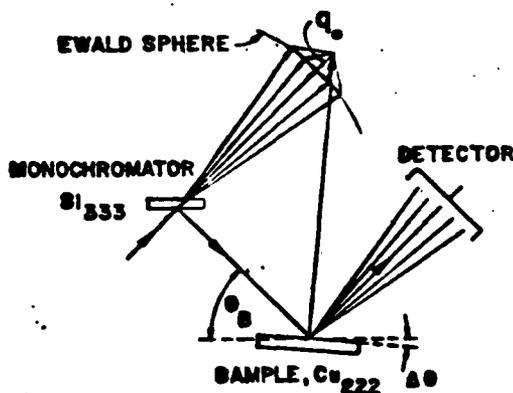
Fig. 1. Range and Damage Profiles.

Fig. 2. Scattering Diagram.

the removal of damage, one of the crystals was annealed at 500°C for 30
minutes and the other crystal at 600°C for 30 minutes. X-ray measurements
were repeated, then the first crystal was annealed at 900°C for 30 minutes.

Results

The scattering measurements made on the implanted crystal and the
unimplanted crystal are shown in Figure 3 in which the logarithm of
normalized intensity is plotted versus the rocking angle. Excess intensity
in the tails of the rocking curve is on the order of a few percent and more
intensity is found on the low rocking angle side. These scattering features
arise from both microalloying of aluminum in copper and point defect
clusters due to ion damage. Clusters of interstitial and vacancy collapse
into sessile dislocation loops whose short-ranged strain fields of the
loops yield diffuse x-ray scattering. The copper-aluminum alloy at the
surface has a larger lattice parameter which in the absence of damage would
give a small Bragg peak on the low angle side of the rocking curve. The
aluminum ion distribution and the damage distribution overlap so that the
two effects combine to produce an asymmetrical diffuse scattering as
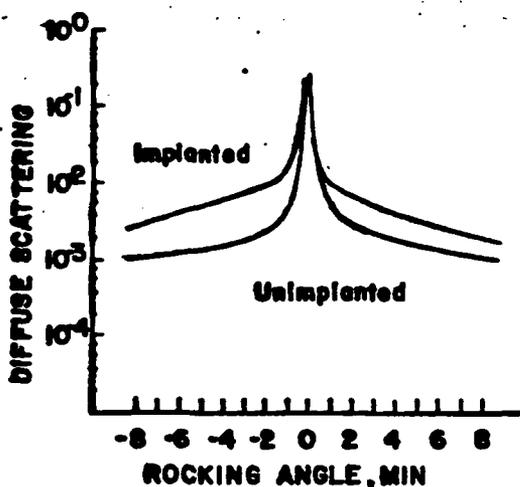discussed below.

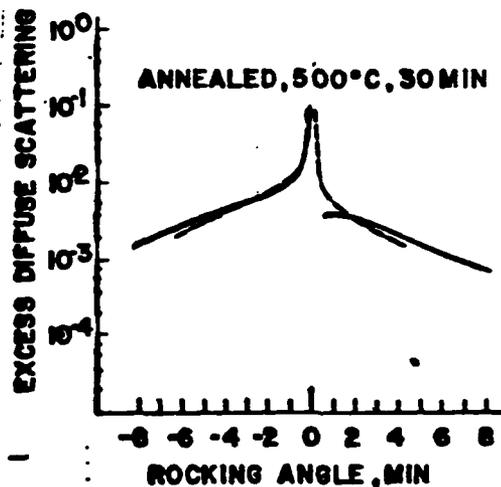Fig. 3. Diffuse scattering from implanted and unimplanted crystals.

Fig. 4. Excess diffuse scattering changes with annealing at 500°C for 30 minutes.

Excess intensity curves are calculated from the difference between the
unimplanted crystal rocking curve and the implanted as well as the implanted
and annealed crystal rocking curves. In Figure 4, excess intensity curves
are shown for the implanted and the implanted-500°C annealed cases. Anneal-
ing at 500°C for 30 minutes produces no appreciable intensity level or
asymmetry change. In Figure 5, excess scattering curves show both a
reduction in excess intensity as well as a loss of asymmetry in the
scattering due to annealing at 600°C for 30 minutes. Not shown are the
results of annealing in 900°C which restored the original condition of the
copper crystal. A significant qualitative finding in these annealing
observations is that the microalloying effect which gives asymmetry in excess
scattering appears to be more readily annealed than dislocation loop effects.
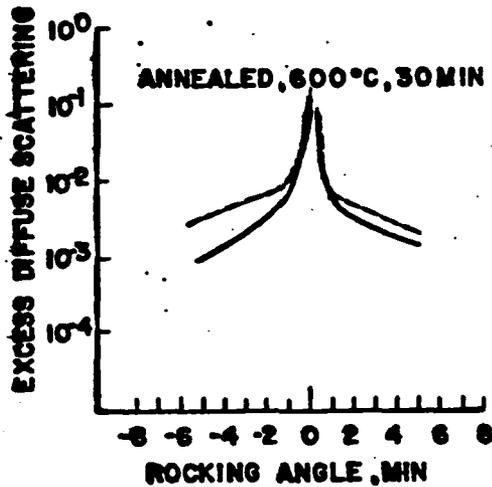
Fig. 5. Excess diffuse scattering changes with annealing at 600°C for 30 minutes.
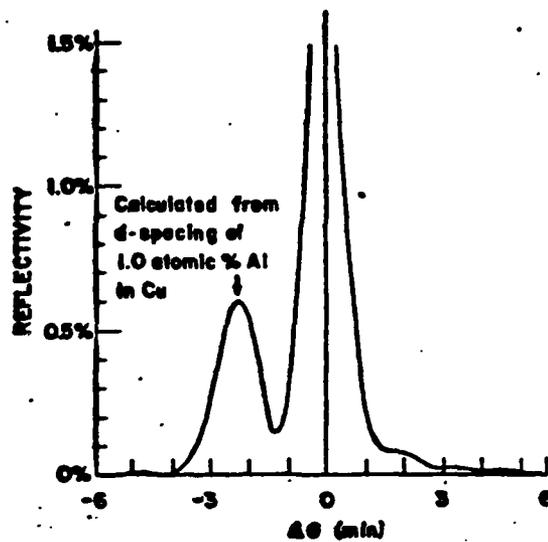
Fig. 6. Dynamical diffraction calculation of scattering from implanted copper.

Calculation of Scattering Effects

The scattering arises from a combination of microalloying and ion damage effects. These effects can be considered separately to provide a perspective on the observed scattering. Microalloying effects are modeled by assuming that the lattice parameter varies with depth according to aluminum content and that the alloyed layer is spacially coherent with the substrate. The resulting diffracted intensity can be calculated using an approach (10) based on an adaption of dynamical diffraction theory described by Klar and Rusticelli (15) for the description of elastic lattice distortion effects. Two coupled differential equations for the real and imaginary x-ray amplitudes are set up to incorporate lattice strain as a function of depth into the crystal. The equations are numerically integrated starting with boundary conditions on the real and imaginary scattering amplitudes at an external surface. Effects rising from the implanted microalloy are calculated by first determining the amplitude components at a depth well below the implanted alloy region. This is done by integrating from the reflecting surface into the crystal using the reflected amplitudes expected at the reflecting surface for an unimplanted crystal. The integration then procedes from the interior to the surface but now with alloying strain effects modifying the integration calculations. Figure 6 shows the calculated reflectivity for the case of a 1 atomic percent alloy at a depth of 1300 Å. A small Bragg peak appears on the low angle side whose position corresponds to a 1 atomic percent alloy and whose intensity is approximately 0.5%. Presuming that the intensity of this peak is in proportion to the ratio of alloy thickness (1300 Å) to penetration thickness $(1/\mu_{cu})$, then the observed intensity should be 0.6%.

The analysis of scattering from radiation damage effects is complicated by the fact that the damaged region coincides with alloyed region created by implantation. The scattering is assumed to arise from the short range strain fields of the loops which give Huang scattering (16) near the Bragg peak

position. Since no distinct Bragg peak has been observed, quantitative analysis of observed scattering is not really valid and one must procede along qualitative directions given below. The analysis of scattering from point defect clusters including sessile dislocation loops of vacancy and interstitial type is concisely reviewed by Larson. (17) Huang scattering intensity around the Bragg peak gives detailed information on cluster density and type, but the scattering intensity is integrated over the Ewald sphere near the Bragg position so as to give an "integral diffuse scattering." The scattering averaged from above and below the Bragg peak is given by (18)

$$I^S (q_o) = \text{constant} \times C_L \left(\frac{b\pi R^2}{V_C}\right) \ln (q_L/q_o)$$

for $q_o \leq q_L$ where $q_o = h\cos\theta\Delta\theta$ with $h = d^{-1}_{hk\ell}$, θ is the Bragg angle and $d_{hk\ell}$ is the $hk\ell$ plane d-spacing. C_L is the density of dislocation loops of radius R with Burgers vector, b, V_C is the unit cell volume in q_L is approximately 1/R. This result can be used to obtain an average loop size, and a determination of loop size distribution and density is possible as well (18).

Analysis and Discussion

No distinct Bragg diffraction peak satellite associated with a implanted microalloy layer is observed. Since radiation damage is concentrated in the alloy layer, the degree of crystalline perfection within the layer is so poor that the dynamical diffraction calculation is simply not appropriate. The Scherrer formula estimate of the kinematic diffraction theory breadth for the implanted layer is approximately 5 times greater than the width calculated by dynamical theory. Thus, any distinct Bragg peak would be broadened into a small general scattering on the low angle side of the rocking curve as observed.

The analysis of the observed intensity in terms of dislocation loop scattering was persued using the approach outlined above. First, the angular position of defect scattering was measured relative to an assumed microalloy Bragg position. This position was calculated on the basis of the lattice parameter for a 1.8 atomic percent copper solid solution. The diffuse excess scattering is plotted versus $\ln(\Delta\theta)$ in Figure 7 and a straight line is seen. From the intercept of the line with the abscissa, q_L was obtained to give an average loop radius of 25 Å. This may be compared to a loop radius of 16 Å found in a similar analysis of neutron irradiated copper at room temperature.

A comparison of the magnitude of measured scattering intensity in the present experiments with a similar experiment (19) on nickel self-ion implantation shows that the observed scattering is within reasonable expected values. 4 Mev Ni ions where implanted into a nickel single crystal to a dose of 5×10^{13} ions/cm^2 at room temperature, although the dose is lower, a comparable point defect generation can be expected because of the higher ion energy. An estimate is made with a modified Kinchen-Pease model (20) for Frenkel pair production:

$$\nu = 0.8 \ E_d/2E_D^{avg}$$

where E_d is the damage energy and E_D^{avg} is the average displacement energy. The ratio of defects produced in Cu by 200 Kev Al ions to the defects produced in Ni by 4 Mev Ni ions is 20 after dose differences are taken into account. Figure 8, which shows the excess scattering intensity, a scattering ratio of approximately 7 is observed. There are several factors which must be considered in comparing dislocation loop scattering intensities.
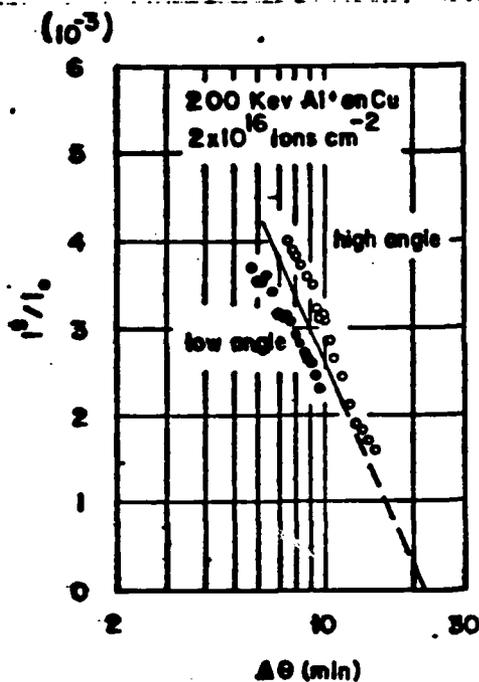
Fig. 7. Excess intensity vs. ln∆θ is plotted to obtain an average loop radius of 25 Å in the implanted sample.
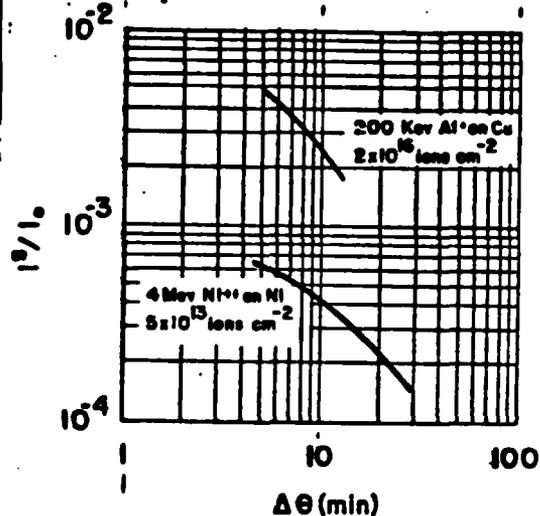
Fig. 8. Comparison of Ni self-ion implantation with Al ion implantation in Cu.

Since the intensity varies as R^4, differences in loop radius between the two cases will affect scattering levels considerably. Agreement between the two cases within a factor of ten is considered satisfactory.

The annealing response in aluminum implanted copper suggests that aluminum migrates into the interior at 600°C and leaves dislocation loops in place although reduced in density. Thus, the damaged state has a degree of stability making the dislocation loops a potentially useful barrier to slip at the surface. At 600°C one can expect removal of loops unless they are stablized by alloying interactions or entanglement. It is not yet possible to assess which factor might be most important.

Conclusions

X-ray diffraction analysis of intensities measured with the double-crystal arrangement has qualitatively shown that a microalloy layer which is heavily radiation damaged is produced by aluminum ion implantation into copper. With the current interpretation, we believe that an alloy layer having a larger lattice parameter will produce a compressive stress on the surface and a tensile stress on the interior as the alloy layer maintains coherency with the substrate. Upon annealing, the aluminum solute leaves the surface layer but radiation damage produced dislocation loops remain, possibly stablized by alloy effects or dislocation entanglement. The beneficial effects of such a surface structure on fatigue crack initiation in polycrystalline copper is discussed in a companion paper.

The diffraction effects seen in alloy implantations is dominated by radiation damage effects. The principal observation which can be used to

deduce surface stress state is assymmetry in the scattering about the substrate Bragg peak and such effects can be seen only in relatively perfect crystals.

Acknowledgments

References

1. E. Y. Chen and E. A. Starke, Jr., "Effects of Ion-Plating on the Low Cycle Fatigue Behavior of Copper Single Crystals," _Mat. Sci. Eng._, 24 (1976) pp. 209-221.

2. B. R. Livesay and E. A. Starke, Jr., "Interactions of Dislocations with Interfaces," _Acta Met._, 21 (1973) pp. 247-254.

3. P. D. Townsend, J. C. Kelly and N. E. W. Hartley, Ion Implantation, Sputtering and Their Application, Academic Press, New York, 1976.

4. G. Dearnaley et al. eds, Ion Implantation, North-Holland Publ. Co.; American Elsevier, New York, 1976.

5. S. Fujishiro, "Improved High Temperature Mechanical Properties of Titanium Alloys by Pt Ion Plating," presented at the Int. Conf. Metallurgical Coatings, San Francisco, April 1978.

6. B. D. Cullilty, "Elements of X-Ray Diffraction," 2nd ed., Chapter 16, Addison-Wesley Pub. Co., Inc., Reading, MA 1978.

7. B. E. Warren and B. L. Averbach, "The Effect of Cold-Work Distertion on X-Ray Patterns," _J. Appl. Phys._, 21 (1950) pp. 595-599.

8. J. E. Thomas, T. O. Baldwin and P. H. Dederichs, "Diffuse X-Ray Scattering in Fast-Neutron-Iradiated Copper Crystals," _Phys. Rev._ 3(4) (1971), pp 1167-1173.

9. B. C. Larson and W. Schmatz, "Huang Diffuse Scattering from Dislocation Loops and Cobalt Precipitates in Copper," Phys. Rev. B 10(8) (1974), pp. 2307-2314.

10. B. C. Larson, C. W. White and B. R. Appleton, "Unidirectional Contraction in Boron-Implanted Laser-Annealed Silicon," _Appl. Phys. Lett._, 32 (12) (1978), pp. 801-803.

11. J. Lindhard, M. Scharff and H. E. Schiott, "Range Concepts and Heavy Ion Ranges," Kgl. Danske Videnskab, Mat.-Fys. Medd. 33 (14) 1963, pp. 1-42.

12. J. Keinonen, M. Hautala, M. Luomajarvi, A. Anttila and M. Bister, "Ranges of ^{27}Al$^+$ Ions in Nine Metals Measured by (p, γ) Resonance Broadening," _Rad. Eff._, 39 (1978), pp. 189-193.

13. K. B. Winterbon, P. Sigmund and J. B. Sanders, "Spatial Distribution of Energy Deposited by Atomic Particles in Elastic Collisions," _Kgl. Danske Videnskab. Selskab, Mat.-Fys. Medd._, 37 (14) (1970), pp. 1-73.

14. K. B. Winterbon, _Ion Implantation Range and Energy Depositon Distributions, Vol. 2, Low Incident Ion Energies._ IFI/Plenum Press, New York, 1975.

15. B. Klar and Rusticelli, "Dynamical Neutron Diffraction by Ideally Curved Crystals," _Nuovo Cimento_, 13B (1973) pp. 249-270.

16. P. H. Dederichs, "Diffuse Scattering from Defect Clusters Near Bragg Reflections," _Phys. Rev. B_, 4 (4) (1971) pp. 1041-1050.

17. B. C. Larsen, "X-Ray Studies of Defect Clusters in Copper," _J. Appl. Cryst._, 8 (1975), pp. 150-160.

18. B. C. Larson and F. W. Young, Jr., "A Comparison of Diffuse Scattering by Defects Measured in Anomalous Transmission and Near Bragg Reflections," _Phys. Rev._, B4 (1971) pp. 1709-1713.

19. J. Narayan and B. C. Larsen, "Defect Clusters and Annealing in Self-Ion-Irradiated Nickel," _J. Appl. Phys._, 48 (11) (1977) pp. 4536-4539.

20. K. L. Merkle, "Defect Production by Energetic Particle Bombardment," pp. 58-94 in _Radiation Damage in Metals_, N. L. Peterson and S. D. Harkness eds, ASM, Metals Park, Ohio, 1976.

APPENDIX B

X-RAY SCATTERING INVESTIGATION OF MICROALLOYING AND
DEFECT STRUCTURE IN ION IMPLANTED COPPER

By

S. Spooner

X-RAY SCATTERING INVESTIGATION OF MICROALLOYING

AND DEFECT STRUCTURE IN ION IMPLANTED COPPER

S. Spooner

Fracture and Fatique Research Laboratory
Georgia Institute of Technology
Atlanta, Georgia 30332

The double-crystal method for x-ray scattering analysis of radiation described by B. C. Larson (1) has been applied to the investigation of aluminum implanted copper. The interpretation of x-ray observations is based on effects of lattice strain in the surface microalloy and the presence of dislocation loops which originate from implantation damage. The copper crystal with a dislocation density less than 10^3 cm/cm^3 was implanted with aluminum to a dose of 2×10^{16} ions/cm^2 with energies up to 200 keV. The response of the implanted crystal to annealing at 500 and 600°C was determined. The quantitative use of the x-ray technique to assess implantation effects and limitations of the technique are discussed.

Introduction

X-ray diffraction is an effective method for analyzing radiation damage particularly for quantitative measurement of lattice strain effects associated with defect clusters (1). In recent years there have been a variety of x-ray diffraction investigations of ion implantation damage produced in single crystals based on double-crystal measurements. Komenou et al (2) observed x-ray scattering resembling Pendellosung interference in rocking curves from Ne^+ -implanted garnet films which Speriosu (3) interpreted according to a kinematic diffraction theory encorporating strain and damage distributions as a function of depth. A fanasev et al (4) have used dynamical theory for calculating the scattering from a silicon crystal with disturbed layers. Yamagishi and Nittono (5) studied Ar^+ ion-implanted copper whiskers with both x-ray topography and a triple-crystal diffraction method to assess lattice strain response with dose and annealing. In the foregoing studies (2-5) no absolute intensity measurements were made so that analysis of structural changes depended mostly upon scattering distribution shape. In the present study, absolute reflectivity measurements are used to study the effects of AL^+ -ion damage in copper due to low energy (200 kev) and high dose (2×10^{16} ions/cm^2) with a double-crystal diffraction method. Both surface alloying and implantation damage are under consideration for their important influence on fatigue crack initation (6) Because radiation damage production of point defect clusters enters our work in a fundamental way, this paper offers an example of the utility of x-ray scattering techniques in radiation damage research.

The principal challenge is this x-ray study was to find an effective x-ray method for investigating the damage and surface alloying effect in an implanted layer which is much thinner than the sampling depth of x-rays. In addition, there was the consideration of which theoretical analysis of scattering intensity would be most appropriate to describe the combined damage and surface alloying scattering effects. This question was approached from two perspectives; (a) use of dynamical theory of diffraction for the analysis of lattice strain due to surface alloying (7,8) and (b) use of kinematic theory for the description if scattering from defect clusters (1). It is shown that the scattering data is dominated by implantation damage defect clusters and that the kinematic theory is most appropriate for the description of scattering in the case at hand. Furthermore, it is shown that a quantitative evaluation of implantation damage can be obtained from the absolute reflectivity measurements made in the double-crystal method.

X-Ray Scattering Models

The implanted region structure is modeled by the superposition of damage produced clusters within a surface alloy layer which has a lattice parameter that is different from the unimplanted substrate. As yet, no single formulation for scattering intensity gives a calculatin of the scattering for the combined defect cluster and lattice distortion effects. Instead, we make a calculation for the case of scattering from a defect-free surface alloy on one hand and a calculation for the scattering from defect clusters in a pure matrix on the other hand. The measured x-ray scattering effects are then used to determine the manner in which the two calculations might be applied to represent the scattering from the implanted layer.

For a surface alloy layer free of defects, dynamical theory of x-ray scattering can be used to calculate the reflectivity of x-rays as a function of crystal rotation in a double-crystal rocking curve. In a two-crystal arrangement, the first crystal which is alloy-free is set to maximum reflectivity. The second crystal is rotated about an axis perpendicular to the scattering plane (defined by the incident and reflected x-ray beams). The resulting reflectivity curve is the convolution to the reflection

characteristic of the first crystal with the reflectivity of the second crystal. Larson (7,8) has adapted for this surface alloy problem a method of calculation used by Klar and Rustichelli (9) for neutron scattering from elastically bent crystals. The reflectivity from a crystal is obtained by the computation of the real amd imaginary components of the complex scattering amplitude of the reflected radiation. Two coupled differential equations - one for real and one for imaginary component - are integrated numerically. The integration is dependent upon initial values of the amplitude components and the variation in the Bragg angle for the crystalline sublayers due to the elastic lattice distortion arising from bending or composition change. Full algebraic development of the theory can be found in papers by Larson and Borhorst (8) and Klar and Rustichelli (9). The equations requiring integration express the derivatives of the real (X_1) and imaginary (X_2) scattering amplitude components with respect to a variable A which is proportional to depth measured relative to the external surface:

$$\frac{dX_1}{dA} = k \ (X^2_1 - X^2_2 + 1) + 2X_2(X_1-y) - 2gX_1 \qquad (1)$$

$$\frac{dX_2}{dA} = -(X^2_1 - X^2_2 + 1) + 2X_1(X_2k+y) - 2gX_2 \qquad (2)$$

where k and g are constants which depend on x-ray absorption and the parameter y contains the misset angle, $\Delta\theta$, for the rocking curve as follows:

$$y = C_1 \ \Delta\theta - C_2 \qquad (3)$$

where C_1 and C_2 are constants dependent on x-ray scattering parameters that are fixed for the Bragg diffraction peak under examination. It is shown (8) that the parameter y can be reexpressed for the case where the lattice parameter varies with A as follows:

$$y = C_1(\Delta\theta + \epsilon(A) \ \tan\theta_B) - C_2 \qquad (4)$$

where the variation of the lattice parameter with depth is contained in the strain function $\epsilon(A)$. In the case at hand, $\epsilon(A)$ is determined by the compostion of the surface alloy as a function of implantation depth.

The method by which the chaṇge in reflectivity due to surface alloying is calculated does not require integration over the entire crystal thickness. Instead, one uses the well known results (10,11) for the reflectivity from a perfect crystal as a starting point. The real and complex components of the scattering amplitude at a set rocking angle are used as initial values for the integration into the interior of the perfect crystal($\epsilon(A) = 0$) to a depth below the implanted ions. Then, the amplitude components at that depth are used as initial values for the integration back to the surface but with the effects of surface alloying, $\epsilon(A)$, now allowed to affect the computation of scattering amplitude. A set of these calculations is done for a range of rocking angles where the reflectivity is calculated from,

$$R(\Delta\theta) = X^2_1 + X^2_2 \qquad (5)$$

where the amplitude components, X_1 and X_2 are evaluated at the reflecting crystal surface. Note that the result is an absolute reflectivity.

Figure 1 shows the results of calculation we have obtained for the case in which a 1 atomic per cent aluminum is implanted in copper to a depth of approximately 1100A°. The lattice parameter expansion used in this calculation was calculated from the data given on linear lattice strain by
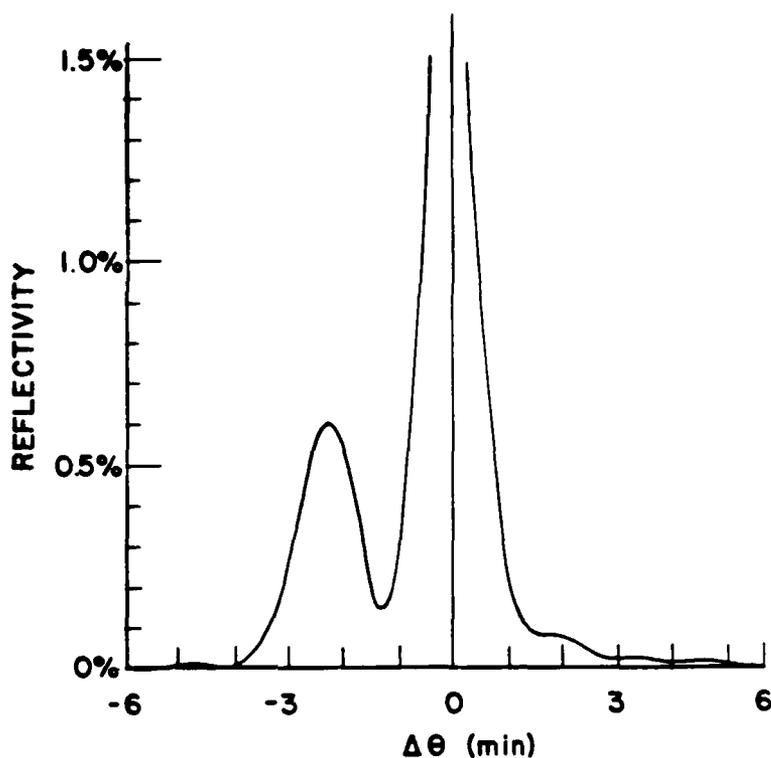
Fig. 1 - Calculated reflectivity from a 1100 Å surface alloy of 1 atomic percent of aluminum in copper. The subsidiary peak appears at an angle appropriate for the lattice parameter of this composition.

Fig. 3

Scattering geometry for the double-crystal method used in this experiment. Upon rocking the crystal the Ewald scattering sphere is swept through the Bragg point. At a fixed crystal setting the diffuse scattering is integrated over a portion of the scattering sphere near the Bragg point.
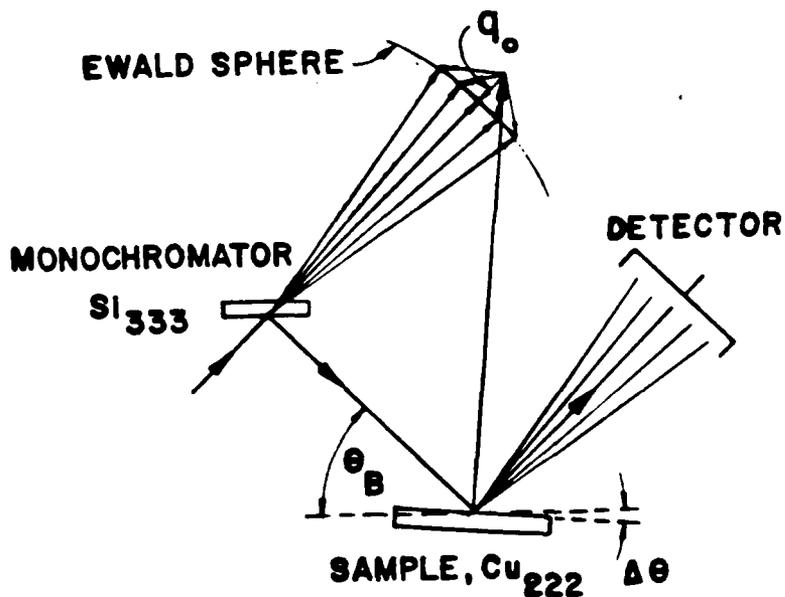
King (12) equal to +0.0626 per atomic percent of aluminum in copper. A sharp subsidiary peak of 0.5% reflectivity is seen at a Bragg angle displaced to a lower angle corresponding to the expanded lattice parameter. The small peak width is approximately 1 minute of are. The reflectivity very nearly equals the ratio of implanted layer thickness to x-ray penetration thickness, $1/\mu_o$, where μ_o is the linear absorption parameter.

Consider now the calculation of the scattering from defect clusters in a crystal of uniform lattice parameter. In this case, Kinematic diffraction theory is used to calculate the scattering intensity from an isolated defect cluster. The scattering resulting from a collection of defects is the sum of these intensities. This implies that no scattering interference occurs between scattering amplitudes coming from each defect. Larson (1) summarizes the calculation of the scattering intensity from defect clusters. The experimental geometry used in our experiments is shown in Figure 2 where the scattered x-rays are recieved into a large detector and to each of the scattering vectors is associated a scattering space vector q going from the Bragg spot (at the top) to the surface of the Ewald scattering sphere. In such an experiment, the intensity is averaged over the scattering space vectors, q. q_o is the shortest vector between the Bragg position and the Ewald sphere at a given crystal setting. The measured intensity is called the integral diffuse scattering. The intensity is measured as a function of rocking angle of the crystal in the same geometry used for measurement of dynamical diffraction effects described above.

The diffuse scattering from dislocation loops measured close to the Bragg peak is attributed to long range strain fields around the loop and is called Huang scattering. Scattering measured farther away from the Bragg peak is attributed to short range strain fields and is termed Stokes-Wilson scattering. The diffuse scattering is distributed about the Bragg position in a way dependent on the precise strain field distribution (1,13). The calculation of integral diffuse scattering requires an averaging of the diffuse scattering over the portion of the Ewald scattering sphere which is close to the Bragg position. (14) For the scattering from loops of radius R, the Huang scattering smoothly joins the Stokes-Wilson scattering at a scattering parameter $q_o = q_2 = 1/R$ where $q_o = h\Delta\theta \cos\theta_B$ with $h = 2\pi/d_{hkl}$, θ_B the Bragg angle for reflection from hkl planes and $\Delta\theta$ the mis-set angle of the rocking curve. A symmetric diffuse scattering cross section is defined

$$\sigma_h^S (q_o) = \tfrac{1}{2} (\sigma_h^S (-q_o) + \sigma_h^S (q_o)) \tag{6}$$

which is obtained by the average of intensities measured symmetrically above and below the Bragg position ($q_o = 0$). The symmetric diffuse cross sections for Huang and Stokes-Wilson scattering are given by,

(Huang) $$\sigma_h^S(q_o)=(r_e f_h e^{-M})^2(h/K)^2 2\pi\tau (b\pi R^2/V_c)^2 \ln(e^{\frac{1}{2}}q_L/q_o) \tag{7}$$

for $q_o < q_1$, and,

(stokes-Wilson) $$\sigma_h^S(q_o)=(r_e f_h e^{-M})^2(h/K)^2 2\pi\tau (b\pi R^2/V_c)^2 q_L^2/2q_o^2 \tag{8}$$

for $q_o > q_1$. r_e is the Thompson electron radius (2.82×10^{-13} cm), f_h atomic scattering factor, e^{-m} is the Debye-Waller factor, $k = 2\pi\lambda$, λ = wavelength, τ is a constant of order 1 which depends on averaging of loop orientations, b Burgers vector, V_c atomic volume. The scattering intensity relative to the incident intensity is given,

$$\frac{I^s(q_0)}{I_0} = \frac{C(R)}{2\mu_0 V_C} \sigma_h^s (q_0) \tag{9}$$

where $C(R)/V_C$ is the density of loops of radius R. From Egs. (7)(8) and (9) one can obtain loop size and density. Note that $(b\pi R^2/V_C)$ equals the number of point defects in the defect cluster.

In summary of the two calculations, the dynamical theory predicts a subsidiary peak which appears at an angle determined by the lattice strain due to alloying. The kinematic theory predicts a diffuse scattering which is proportional to the number and size of loops. Both calculations give the absolute reflectivity with no adjustable parameters other than those describingthe structure. The dynamical thoery calculation depends on the assumption that the surface alloy is crystallographically coherent with the unalloyed crystal. The limit to the kinematic theory is likely to be found with very high defect cluster densities where interference between diffuse scattering amplitudes may occur.

Experimental

The calculated strain scattering effects must be measured at small angles near the Bragg diffraction peak of the unaffected crystal. The implant affected region is less than 1 micron and the pentration depth is approximately $1/\mu_0 = 22$ microns. It is required that the bulk of the crystal be perfect (mosaic spread less than 1 minute) in order that the small scattering effects can be measured near the Bragg peak. Furthermore, it is required to subtract a sigificant background due to the tails of the bulk crystal Bragg peak in order to determine the diffuse scatterin intensity due to surface alloying and defect clusters. A convenient approach to this measurement is to translate the crystal between an implanted and un-implated area on the sample crystal. Crystals used in these studies were provided by F. W. Young of ORNL. The crystals were grown by Bridgman technique, wt to orientation, then annealed at a few degrees below the melting point for two weeks. The crystal pieces were hardened by neutron irradiation and then further cut and shaped by chemical cutting methods.[15] The dislocation density measured by etch pit techniques was less than 10^3 cm^{-2} after shaping processes were complete.

The two-crystal arrangement consisted of a silicon crystal fixed to diffract the Cu K_α radiation onto the implanted copper crystal. The (333) d-spacing (1.0451 Å) of silicon happens to match the (222) d-spacing (1.0436Å) of copper very well so that the system is well focussed to give a narrow rocking curve width. The copper crystal is initially aligned to give a sharp maximum in the rocking curve by adjusting the (111) normal about an axis in the scattering plane (defined by the incident and scattered beams). When properly adjusted, the full width at half-maximum (FWHM) of the copper rocking curve is 12.5 arc-sec. The crystal is mounted on a goniostat which can be translated in the plane of the crystal surface so that rocking curves can be made from the implanted area and masked unimplanted areas. In a typical run, the copper crystal is rocked about an axis perpendicular to the scattering plane at a rate of 5 to 20 arc-sec per minute while x-ray intensities are recorded continuously at 10 second intervals. The x-ray detector has an active receiving area of 5 cm^2 at a distance of 8 cm so that the subtended soild angle (0.08 steradians) intergrates the scattering over a large portion of the Ewald scattering sphere in the vicinity of the 222 Bragg peak of copper.

The implantation of aluminum into copper was chosen for these experiments because the ion penetration was favorable and the microalloy concentration

was well below the solubility limit of the aluminum in copper. The details of implantation are given elsewhere. (6) The implanted layer was 1200 Å (16) thick with a composition of 1.8 atomic per cent. The distribution of damage over the alloy thickness was estimated on the basis of calculations by Fritzsche (17) and Winterbon. (8) The alloy distribution (solid line) and the damage profile (dashed line) are shown in Figure 3.

Fig. 3

Distribution of implanted Al$^+$ ions (solid) and the energy deposition (dashed) for the implantation of 2×10^{16}ion/cm^2 with energies upto 200 keV. Note that damage is concentrated toward the surface.
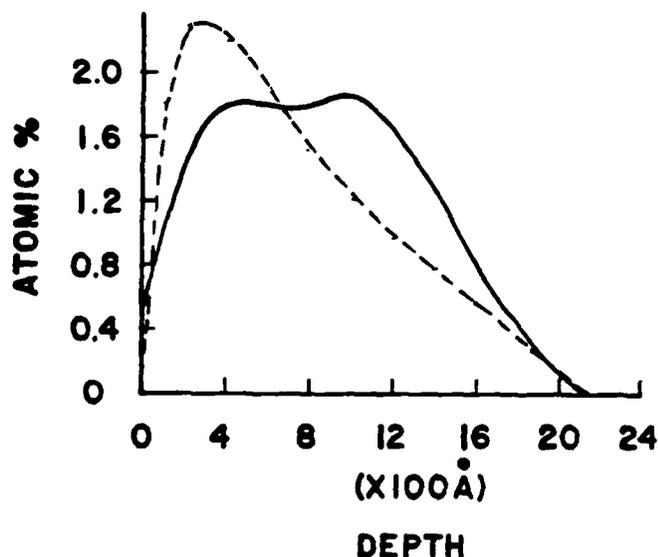
Annealing of the specimens was performed as a means to differentiate the sources of scattering in the implanted layers. The crystals were placed in a vacuum of 10^{-8} Torr at 500°C, at 600°C, and 900°C for 30 minutes. Annealing at 900°C restored the original structure as seen in the rocking curves.

Results and Discussion

The rocking curves for unimplanted copper and for aluminum implanted copper were measured on the same crystal. These cruves are shown in Figure 4.

Fig. 4

Rocking curves are shown for the implanted (upper) and unimplanted(lower) crystal. The scattering is expressed as a fraction of the incidnet beam intensity. Note the larger scattering at low angles.
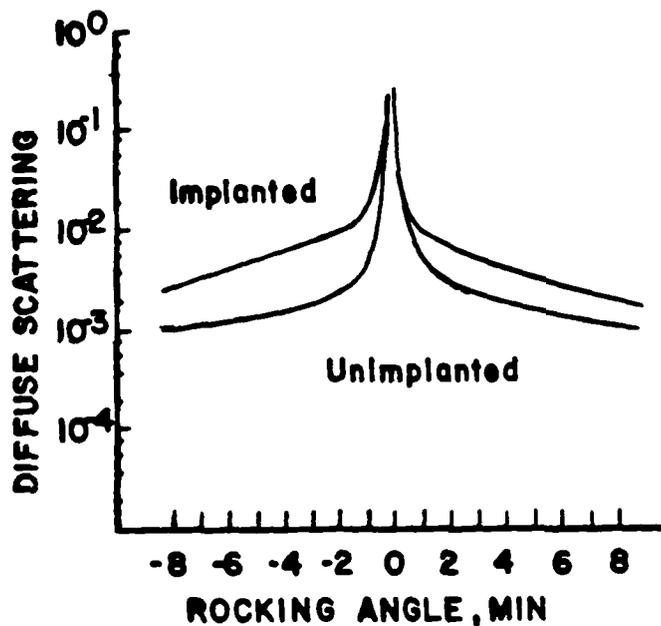
The diffuse scattering from the implanted crystal is more intense on the low angle side of the Bragg peak position. The excess diffuse scattering is calculated by subtraction of the unimplated rocking curve intensity from the corresponding intensity in the implanted crystal. The excess diffuse scattering for the implanted crystal is shown in Figures 5 and 6 as a dashed line. The effect of 30 minute anneals on the excess diffuse intensity is shown in Figure 5 for annealing at 500°C and in Figure 6 for annealing at 600°C.

Fig. 5

Excess diffuse scattering intensity for the sample before annealing (dashed) and after annealing (solid) at 500°C is shown. Note that little change in the general level and distribution of the excess intensity occurs upon annealing.
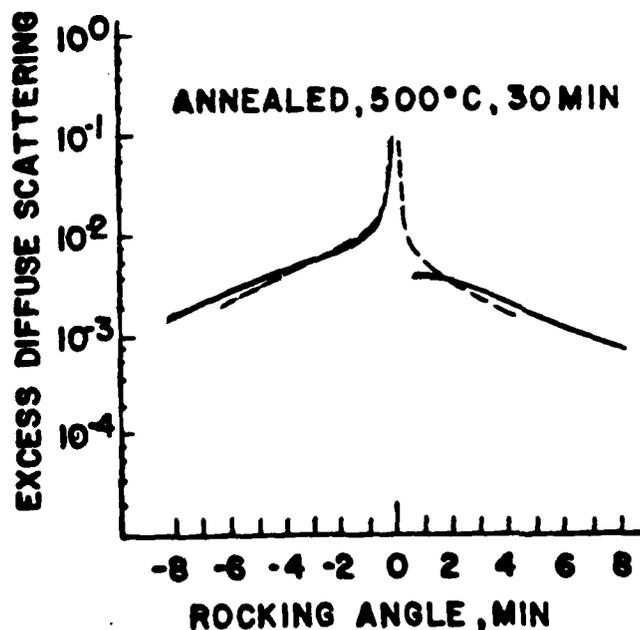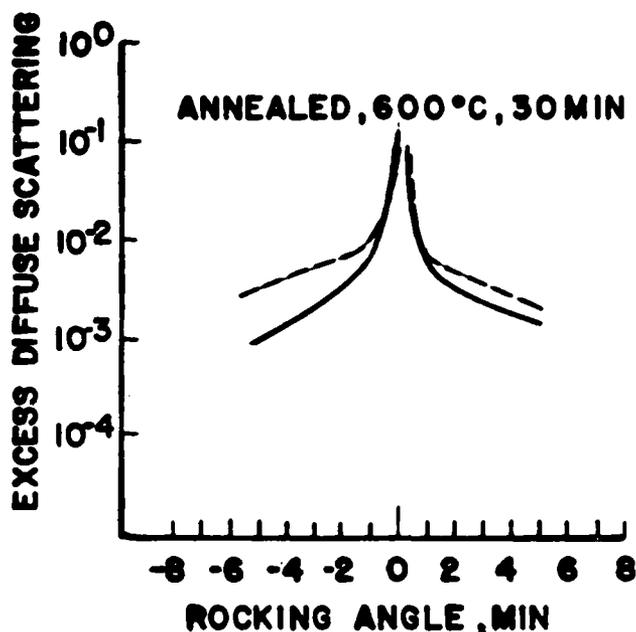
Fig. 6.

Excess diffuse scattering
intensity for the sample be-
fore annealing (dashed) and
after annealing (solid) at
600°C. The level and the
distribution of the excess
intensity has changes as a
result of the annealing at
this temperature.

No large change due to annealing occurs at 500°C while for annealing at
600°C, there is a reduction of scattering and the scattering becomes more
symmetric with respect to the Bragg peak position.

The observation of a higher diffuse scattering at low rocking curve
angles can be attributed to the fact that implanted aluminum expands the
copper lattice so that Bragg scattering from the implanted region occurs at
a lower angle than that for the unimplanted material. The composition of
the implanted layer was estimated to be 1.8 atomic per cent. The resulting
Bragg position would be displaced to lower angle by 4.2 minutes for the 222
reflection from the copper alloy layer.

No subsidiary peak is seen in the rocking cruve data which indicates
that conditions for the dynamical diffraction from the surface alloy do not
apply. Kinematic theory for Bragg scattering from an incoherent microalloy
layer of 1100 Å predicts a rocking curve width about 9 minutes (compare for
example the Scherrer width (19)). The kinematic intensity relative to the
dynamical subsidiary peak would be reduced in proportion to the ratio be-
tween the two peak widths. This suggests that if the implanted layer loses
strict coherence with the unimplanted material, the Bragg diffraction
intensity from the layer would be relative small and spread out on the scale
of these rocking curve measurements.

The diffuse scattering seen on both sides of the main Bragg position
can be compared to calculations of the scattering from dislocation loops.
Figure 7 the excess diffuse scattering is plotted versus the log of the
rocking angle according to Egn. (7) for Huang loop scattering. The rocking
angle was measured relative to the supposed Bragg position for the alloy.
Although there is a displacement between the two sets of points, the average
of the high angle and low angle intensity is close to a straight line which
yields an estimated loop diameter of 25Å.

(10^{-3})

Fig. 7

The excess diffuse scattering from the implanted crystal is plotted versus $\ln(\Delta\theta)$ for the intensity above and below the Bragg position assumed to apply for the implanted region of the crystal.
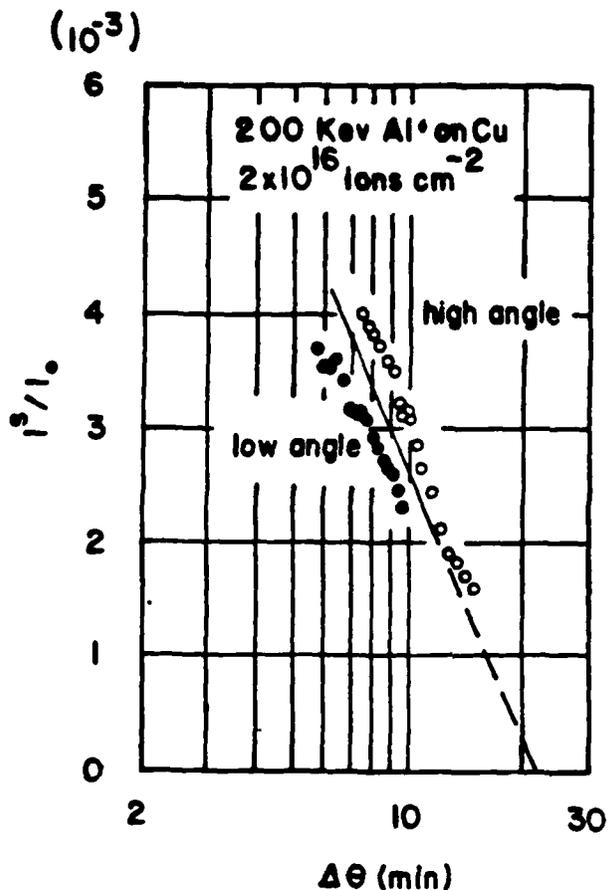
An estimate of the density of loops can be made by comparing measured reflectivity with Eqn. (9). We use a loop radius of 30Å and a reflectivity of 1% at $\Delta\theta$ = 2 minutes. Substitution of appropriate constants into Eqn. 9 for a 30Å loop size gives

$$I^S(qo)/I_0 = 6.1 \times 10^{-21} \frac{C}{V_v} \ln(44/\Delta\theta \text{ (min)})$$

from which a value of C/V_c is 5.3×10^{17} loops/cc. (The loops are concentrated by a factor of 200 in the implanted layer since the above calculation assumes the loops to be uniformly distributed).

The failure to observe a sharp Bragg peak associated with the implanted aluminum and the general agreement with scattering levels calculated for loop scattering point to the conclusion that the kinematic theory for diffraction from an implanted crystal is most appropriate. The annealing at $600°C$ produces symmetrical scattering which suggests that most of the aluminum is removed from the region where loops persist. Thereby, the loop scattering now originates in essentially pure copper. The role of aluminum is seen as simply expanding the lattice in a region which, by virture of severe damage, is no longer strictly coherent with the un-implanted crystal.

Conclusions

Analysis of x-ray diffraction in aluminum ion implanted copper suggests that defect cluster scattering dominates the observed rocking curve intensity. Alloying in the implanted layer contributes through a shifting of the diffuse scattering to lower angles due to the fact that the defect clusters are formed in a region of aluminum-expanded lattice. The formation of a distinct peak predicted by dynamical diffraction theory does not occur probably because spatial coherency between the alloy layer and the substrate is lacking due to severe lattice damage. Problems in the analysis of scattering remain in the area of (1) formulating a model of combined alloying and defect cluster scattering and (2) description of very high defect cluster scattering. Nevertheless the simplistic interpretation of x-ray scattering observation provides useful insights into the type and quantity of damage as well as the annealing response of the implanted structure.

Acknowledgements

References

1. B. C. Larson, "X-ray Studies of Defect Clusters in Copper", J. Appl. Cryst 8. pp. 150-160 (1975).

2. K. Komenou, I. Hirai, K. Asama and M. Sakai, "Crystalline and Magnetic Properties of an Ion-Implanted Layer in Bubble Garnet Films", J. Appl. Phys 49 pp. 5816-5822 (1978).

3. V. S. Speriousu, H.L. Glass and T. Kobayashi, "X-ray Determination of Strain and Damage Distributions in Ion-Implanted Layers", Appl. Phys. Lett. 34, pp. 539-542 (1979).

4. A. M. Afanasev, M. V. Kovalchuk, E. K. Kovev and V. G. Kohn, "X-ray Diffraction in a Perfect Crystal with Disturbed Surface Layer", Phys. Stat. Sol. (a) 42, pp. 415-422 (1977).

5. H. Yamagishi and O. Nittono, "X-ray Study on Lattice Defects in Ar$^+$ Ion Implanted Copper Whiskers", Nippon Kinzokv Gakkaishi 43, pp. 689-695 (1979) (Abstract in English).

6. S. Spooner and K. Legg, "X-ray Diffraction Characterization of Aluminum Ion Implanted Copper Crystals" paper presented at Materials Research Society Meeting, Cambridge, Mass., Nov. 1978.

7. B. C. Larson, C. W. Shite and B. R. Appleton, "Unidirectional Contraction in Boron-Implanted Laser-Annealed Silicon", Appl. Phys. Lett. 32 (1978) pp. 801-803.

8. B. C. Larson and J. F. Barhorst, "X-ray Study of Lattice Strain in Boron Implanted Laser Annealed Silicon", submitted for publication, (October, 1979).

9. B. Klar and F. Rusticheili, "Dynamical Neutron Diffraction by Ideally Curved Crystals", Nuovo Cimento, 13B (1973) pp. 249-270.

10. B. E. Warren, "X-ray Diffraction", Chapter 14, pp. 315-354, Addison-Wesley, Reading, Mass. (1969).

11. W. H. Zachariasen, "Theory of X-ray Diffraction in Crystals", Chapter 3, pp. 83-155 (esp. 140-147), Dover Publications, New York (1967).

12. H. W. King, "Quantitative Size-Factors for Metallic Solid Solutions", J. Mat. Sci 1 (1966) pp. 79-90.

13. B. C. Larson and W. Schmatz, "Huang-Diffuse Scattering from Dislocation Loops and Cobalt Precipitates in Copper", Phys. Rev. B 10, (1974) pp. 2307-2314.

14. B.C. Larson and F. W. Young, Jr., "A Comparison of Diffuse Scattering by Defects Measured in Anomalous Transmission and Near Bragg Reflections", Z. Naturtorsch 28a (1973) pp. 626-632.

15. F. W. Young, Jr., "Etch Pit Studies of Dislocations in Copper Crystals Deformed by Bending. I. Annealed Crystals. II. Irradiated Crystals", J. Appl. Phys. 33 (1962) pp. 3553-64.

16. J. Keinonen, M. Hautala, M. Luomajari, A. Anttila and M. Bister, "Ranges of $^{27}AL^+$ Ions in Nine Metals Measured by (p,γ) Resonance Broadening", Rad. Eff. 39 (1978) pp. 189-193.

17. C. R. Fritzche, "A Simple Method for the Calculation of Energy Deposition Profiles from Range Data of Implanted Ions", Appl. Phys 12 (1977) pp. 347-353.

18. K. B. Winterbon, "Ion Implantation Range and Energy Deposition Distributions, Vol. 2, Low Incident Ion Energies, IFI/Plenum Press, New York (1975).

19. B. D. Cullity, "Elements of X-ray Diffraction", 2nd ed., Chapter 16, Addision-Wesley Pub Co., Inc. Reading, MA (1978).

APPENDIX C

THE EFFECT OF ALUMINUM ION IMPLANATION ON THE FATIGUE CRACK
INITIATION OF POLYCRYSTALLINE COPPER

By

A. Kujore
S.B. Chakrabortty
E.A. Starke, Jr.
and
K. O. Legg

First line of text (for other than title page)

THE EFFECT OF ALUMINUM ION IMPLANTATION ON THE FATIGUE

CRACK INITIATION OF POLYCRYSTALLINE COPPER[+]

A. Kujore, S.B. Chakrabortty, E.A. Starke, Jr.
Fracture and Fatigue Research Laboratory
and
K.O. Legg
School of Physics
Georgia Institute of Technology
Atlanta, Georgia 30332

The effect of Al ion implantation on the low cycle and high cycle fatigue behavior of polycrystalline copper has been investigated. The cyclic stress strain response, stress-life relationship and fatigue crack nucleation behavior of implanted copper are compared with unimplated copper.

The ion implantation did not seem to effect the monotonic yield stress, but did decrease the extent of work hardening in the low strain range. A similar decrease was observed in the cyclic hardening behavior. Al ion implantation produced a significant improvement in fatigue life for both strain and stress controlled tests. This improvement is associated with modifications of the deformation behavior in the surface and near-surface regions of the implanted copper, and its subsequent effect on fatigue crack initiation.

Introduction

The fatigue process may be divided into two stages, crack initiation and subsequent crack propagation. Microcracks usually form at the surface of a material due to cyclic straining, and link-up and growth of these microcracks into a major fatal crack may be termed the initiation stage. A major factor in the initiation of fatigue cracks concerns slip processes at the surface and these are considerably influenced by the surface condition. It is well known that gross surface alterations like shot peening and case hardening can improve fatigue life, and recent results have shown that small surface alterations can also have a considerable effect on fatigue behavior. Chen and Starke (1) studied the effect of ion-plated coatings of copper, nickel, and silver on the low cycle fatigue properties of copper single crystals. They concluded that the ion-plating process itself does not significantly change the cyclic flow stress, but the stacking fault energy of the coating material effects crack initiation by influencing the topography of the slip bands on the surface.

It is unclear whether similar small surface modifications of poly-crystalline samples will produce a change in cyclic life similar to that observed for single crystals. Changes in the deformation behavior of surface grains may be produced by minor surface alterations; however, fatigue cracking of polycrystalline materials may be totally controlled by grain boundary events. The current research was undertaken to elucidate these points. This paper concerns a study of the effect of aluminum ion implantation on the low cycle and high cycle fatigue properties of polycrystalline copper.

Experimental

Cold drawn polycrystalline rods, having 0.03 wt.% oxygen as the major impurity were supplied by the Southwire Company, Carrollton, Georgia. Low and high cycle fatigue specimens were machined from the rods and subsequently annealed for one hour in vacuum at 810°K, ground and hand polished with billiard cloths impregnated with 0.3 μm alumina, and finally electropolished in a nitric-methonal solution. The cylindrical low cycle fatigue samples had a gage section approximately 10 mm long by 3.8 mm diameter, and the hour-glass-shaped high cycle fatigue samples had a minimum diameter of 3.5 mm. Some specimens were sputter cleaned by argon ions at 2.0 KV. Others were implanted with 100 KeV Al^+ ions to a dose of 5×10^{19} ions/m^2. To insure uniformity of implantation, the specimens were rotated in the beam which was scanned across an aperature spanning the gage length. Fatigue tests of Al^+ ion implanted and un-implanted samples were conducted on a servohydraulic closed-loop testing machine, in laboratory air, at 298°K. Low cycle fatigue measurements were made using constant total strain control with a saw-tooth wave form at a strain rate of 5×10^{-4}/sec. Stress control, high cycle fatigue tests were made using a frequency of 10 Hz. Optical and electron microscopy were used to characterize the deformation behavior.

Results

Stress/Strain Response: Al^+ ion implantation did not change the mono-tonic yield stress of polycrystalline copper. However, a small but statistically significant difference between monotonic hardening in the low strain range was observed with the ion-implanted material showing a lower degree of hardening. The monotonic stress-strain curve can be described mathematically by the Lüdwik relationship, $\sigma = \sigma_0 + K \epsilon_p^n$, where σ_0 is the yield stress, ϵ_p the plastic strain, n the strain hardening exponent and K the stress increament at $\epsilon_p = 1$. Figure 1, which is a
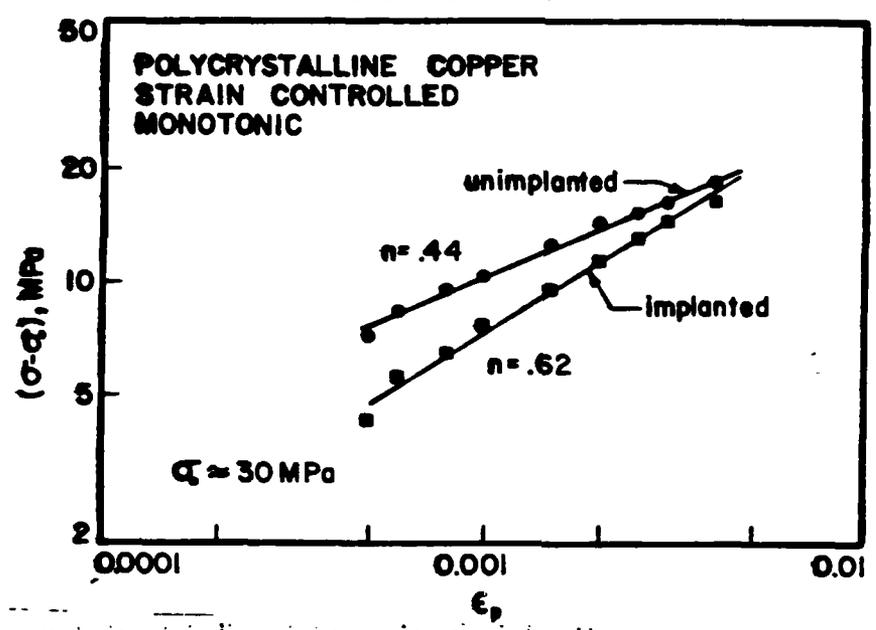
Figure 1. Monotonic stress-strain curves for Al-ion implanted and
unimplanted polycrystalline copper

plot of $\ln(\sigma-\sigma_0)$ versus $\ln \dot{\varepsilon}_p$, illustrates the difference in monotonic
hardening behavior as a function of plastic strain.

Considerable cyclic hardening was observed for both implanted and
unimplanted samples at all strain amplitudes, Figure 2. "Waistometer-type
hardening" (2) was recorded subsequent to the saturation state. However,
since this is an effect of the testing procedure and not a material
characteristic, this portion was deleted and replaced by dotted lines.
Both unimplanted and implanted copper showed cyclic hardening behavior
typical of annealed fcc materials: initial rapid hardening followed by a
saturation stage. The relationship between cyclic stress and plastic strain
can be described mathematically by a power function similar to Lüdwik
relationship, (3) i.e., $\sigma_a - \sigma_0 = \sigma_k' (\Delta\bar{\varepsilon}_p/2)^{n'}$, where σ_0 is the stress for
$\Delta\varepsilon_p/2 = 0$, σ_a is the stable stress amplitude, $\Delta\varepsilon_p/2$ is the plastic strain
amplitude, n' is the cyclic strain hardening exponent, and σ_k' is the cyclic
strength coefficient. Figure 3, which is a plot of $\ln(\sigma_a - \sigma_0)$ versus $\ln$
$(\Delta\varepsilon_p/2)$ shows that, analogous to the monotonic behavior, the implanted
material cyclically hardens less than the unimplanted material.

Strain-Life Curves (LCF): Figure 4 compares the strain-life curves
(Coffin-Manson plots) for the implanted and unimplanted polycrystalline
copper. Coffin (4) and Manson (5) independently proposed a relationship
between the plastic-strain amplitude and the cycles to failure of the form:
$\Delta\varepsilon_p/2 = \varepsilon_f' (2N_f)^c$ where ε_f' is the fatigue-ductility coefficient, $2N_f$ is
the number of reversals to failure, and c is the fatigue ductility
exponent. Al^+ ion implantation significantly improves the cyclic ductility,
as noted by an increase in ε_f', but also increases the absolute value of
the cyclic ductility exponent.
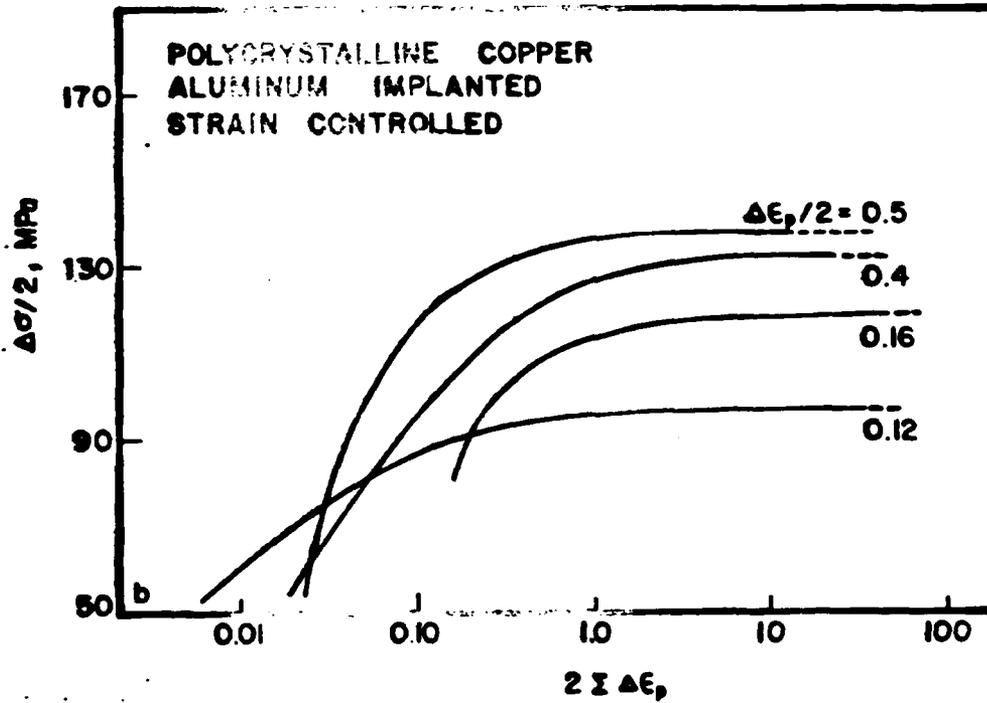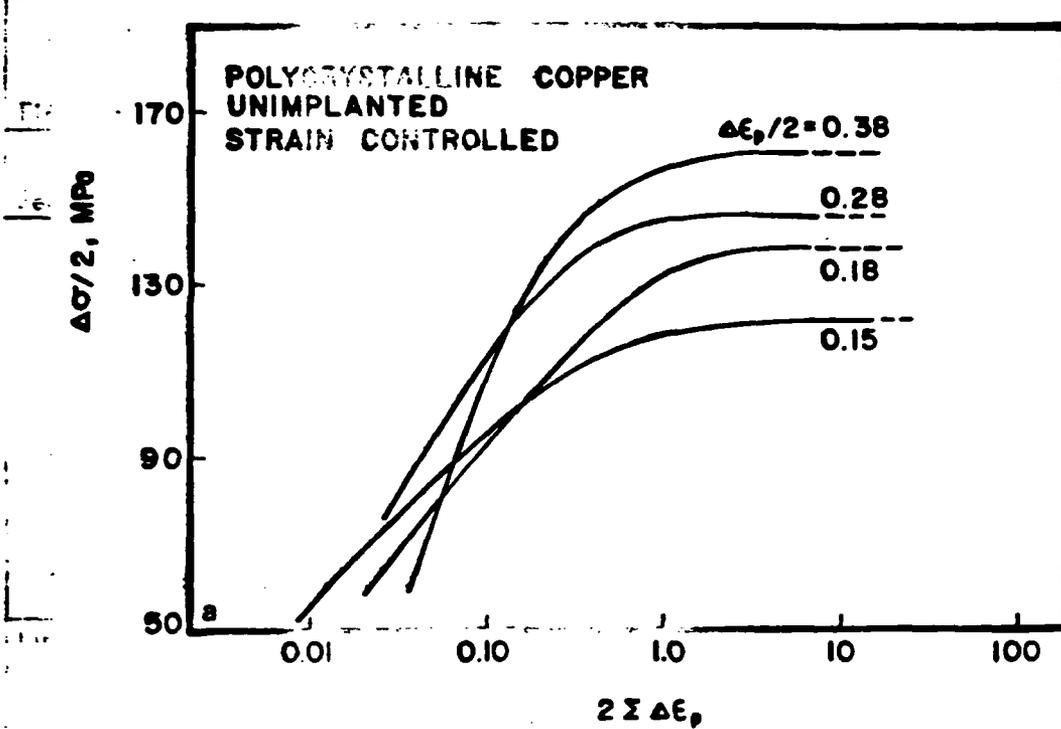
Figure 2. Cyclic stress response curves obtained during strain controlled LCF testing.

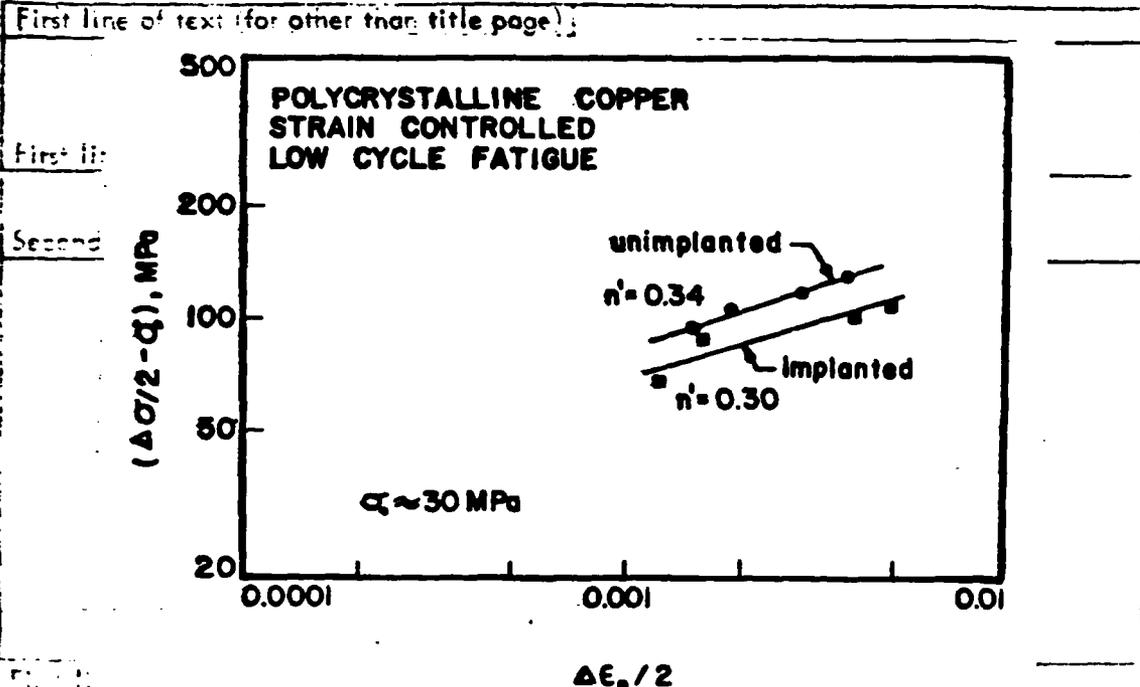First line of text (for other than title page)

Figure 3. Cyclic-stress-strain curves for Al-ion implanted and
unimplanted polycrystalline copper.
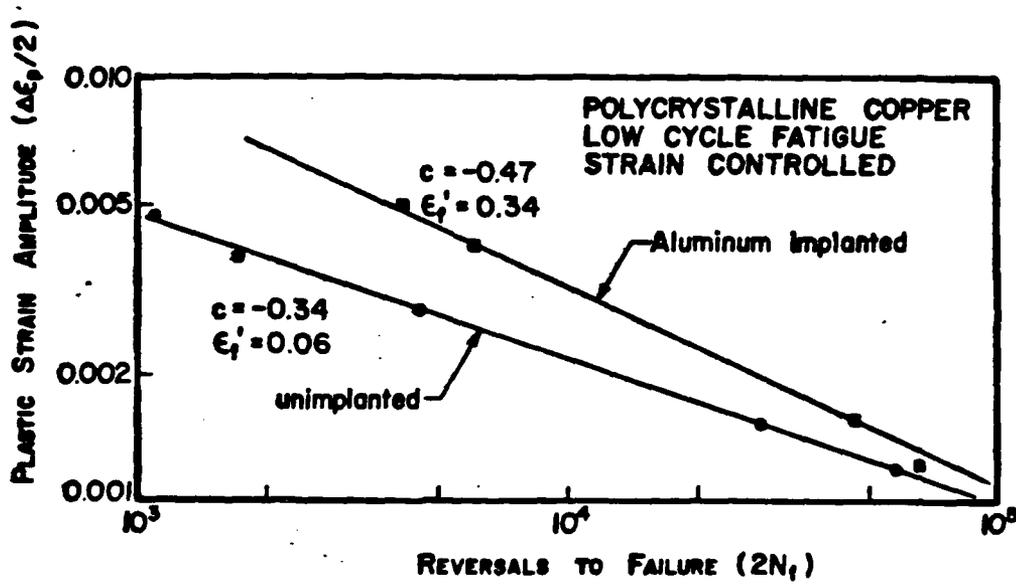

Figure 4. Strain-life curves for Al-ion implanted and unimplanted
polycrystalline copper.

Authors' name   Kujore

5⏀ for final size: 6" x 9" book
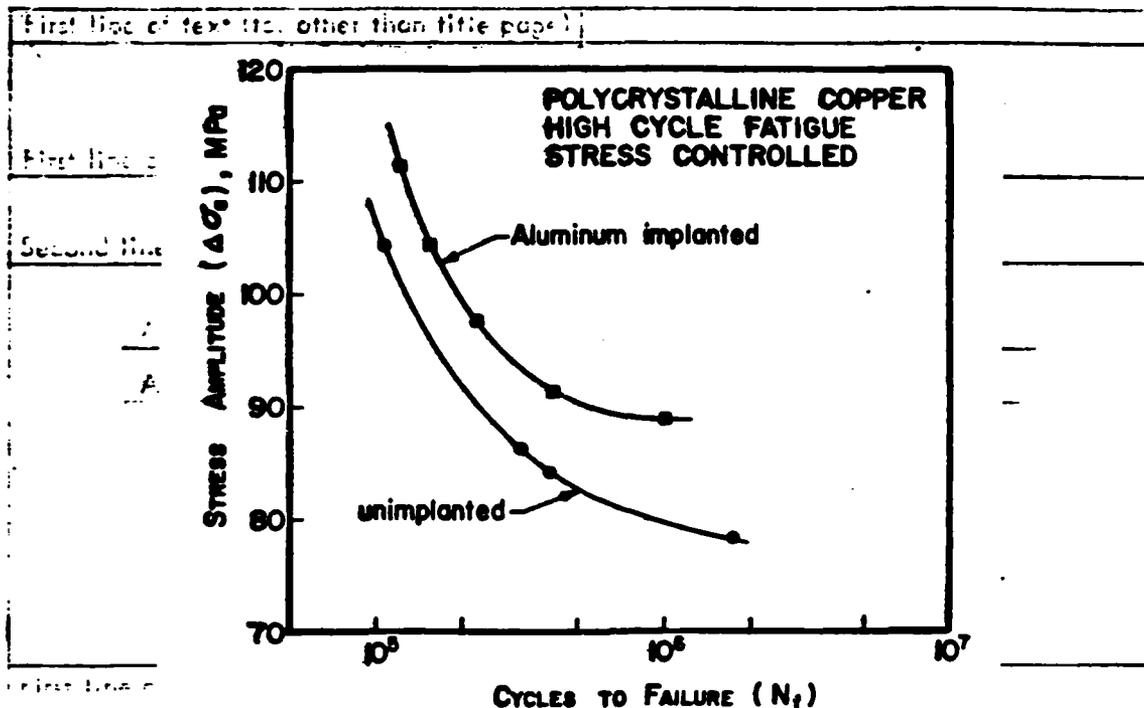First line of text (i.e. other than title page)
First line 1
Second line

Figure 5. Stress-life curves for Al-ion implanted and unimplanted polycrystalline copper.

Stress-Life Curves (HCF): Figure 5 shows the effect of Al^+ ion implantation on the high cycle fatigue behavior of polycrystalline copper. Significant improvement in the high cycle fatigue life is observed, and the improvement is greatest at the lower stresses.

Cyclic Surface-Deformation: Figure 6 compares the surface slip markings of Al^+ ion implanted and unimplanted LCF specimens. It appears that coarse persistent slip bands (PSB) with associated intrusion/extrusions form in both cases. However, the propensity of coarse PSB formation is higher for the unimplanted copper, and somewhat finer, more homogeneous slip appears to be favorable for the implanted material. This results in more PSB cracking for the unimplanted copper, although extensive grain boundary cracking is present in both materials. The grain boundary cracking is associated with surface rumpling resulting from incompatibility of coarse deformation in neighboring grains. The surface rumpling and associated grain boundary cracking is more evident in the unimplanted copper. Surface studies showed that microcrack link-up is also easier in the unimplanted material due to the higher frequency of microcracks in the grain interiors.

Figure 7 shows areas of intense slip markings on the high cycle fatigue samples. It appears that the propensity of PSB formation is quite high in the surface grains having heavy deformation. Cracking associated with these PSB's is also evident. No distinction could be made between the surface slip markings of the two materials. Unlike the LCF surface analysis, surface studies of the HCF samples were made after fatigue failure had occurred. Because of life differences the implanted material had undergone a considerably larger extent of fatigue cycling for the constant stress-amplitude tests.
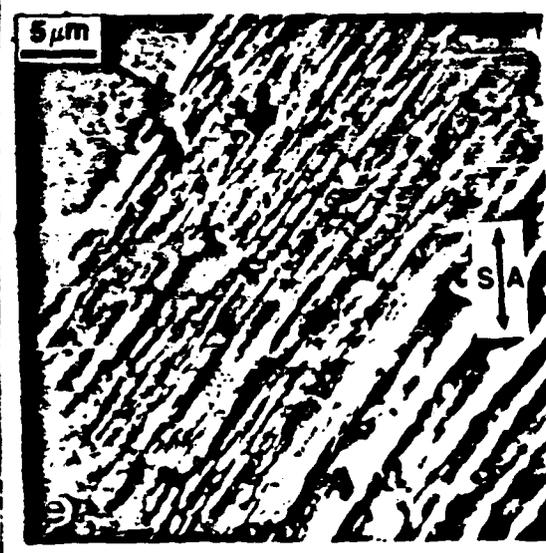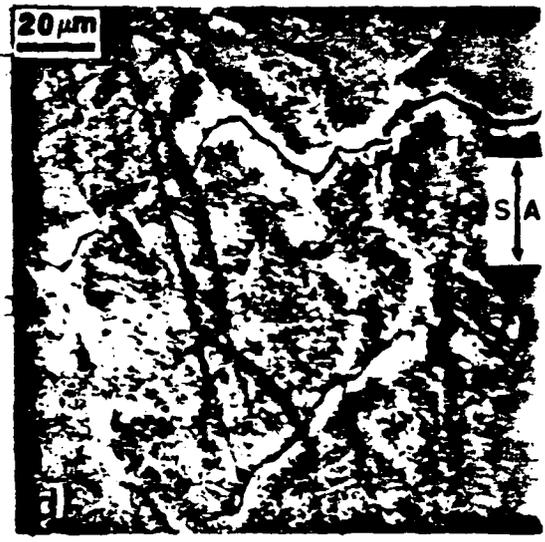
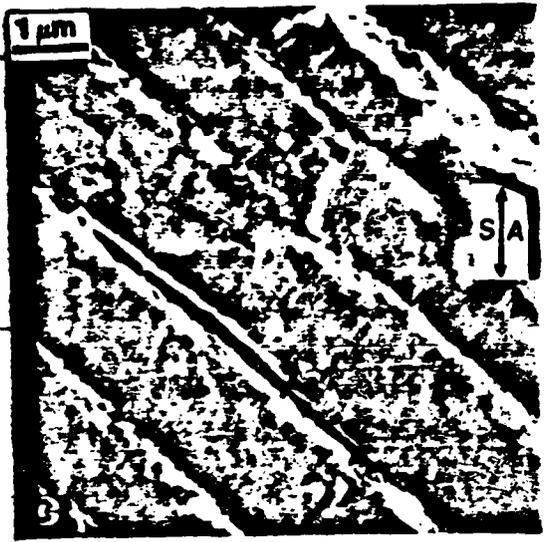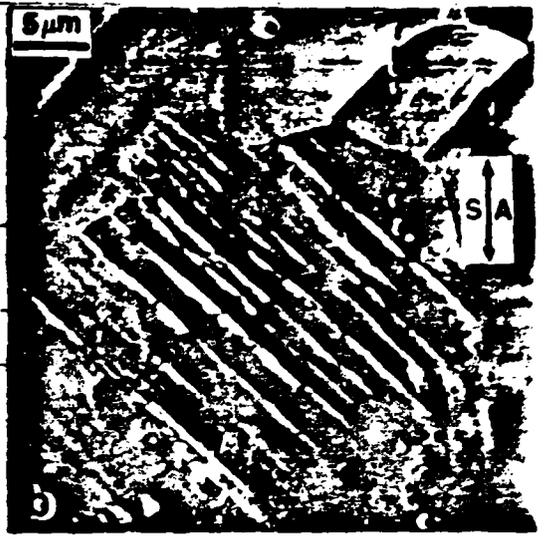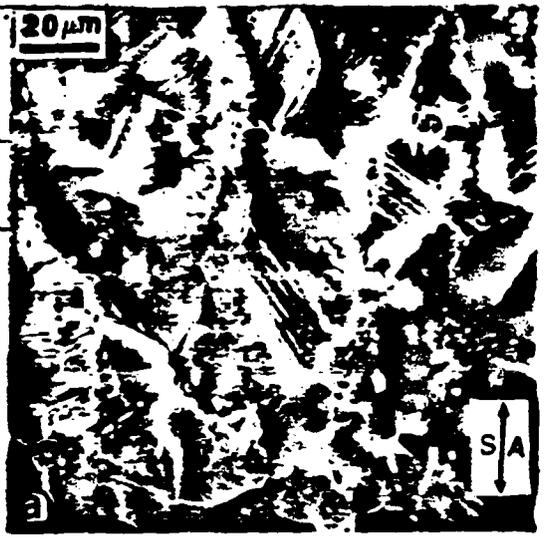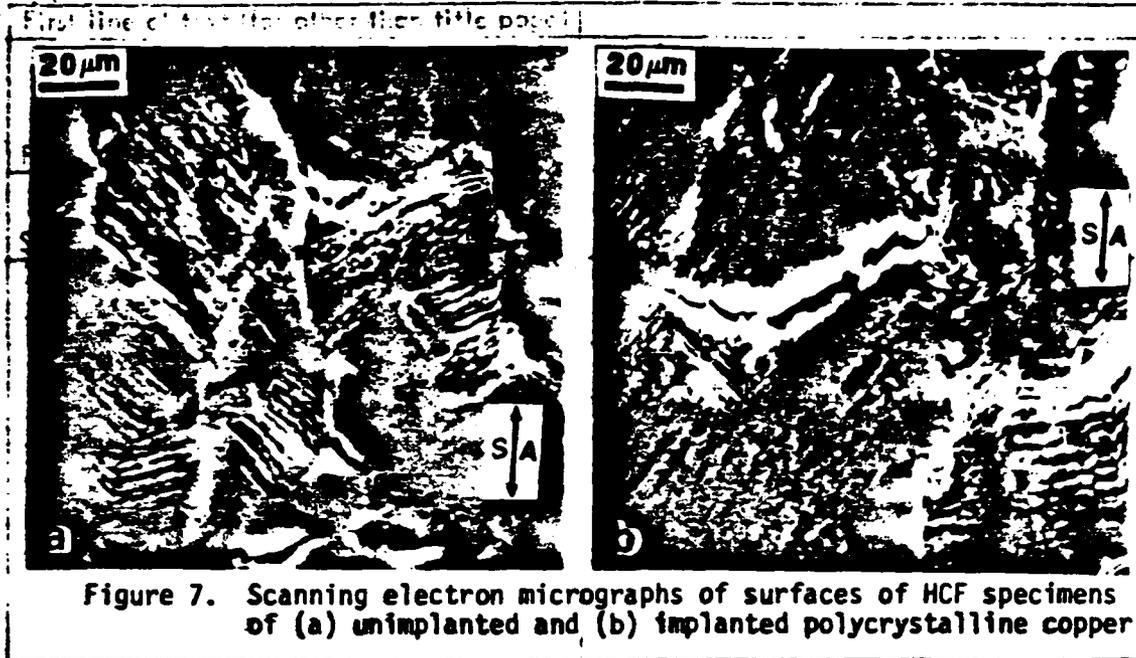Figure 6. Scanning electron micrographs of surfaces of LCF specimens of (a)(b)(c) unimplanted, and (d)(e) implanted polycrystalline copper.

Figure 7. Scanning electron micrographs of surfaces of HCF specimens
of (a) unimplanted and (b) implanted polycrystalline copper.

Discussion

The observations made here are results of our preliminary
investigations. In depth studies are underway to elucidate some of the
points discussed here and will be presented in future publications.

X-ray diffuse measurements by Spooner and Legg (6) and theoretical
considerations may be used to estimate the surface modification made by
ion-implantation. In our case, the ion beam is broader than the diameter
of the fatigue specimens which are rotating cylinders. This is expected to
produce an aluminum concentration profile with a peak of 0.7 wt. % at a
depth of 55 nm with a full width at half maximum of 85 nm as against 70 nm
for both parameters in normal incidence implantation (6) . The resulting
damage profile (6) is expected to be similar but may be slightly displaced
with respect to the concentration profile. Sputter cleaning of the
unimplanted samples may have also created some damage in the surface layer.
However, since the helium ions used for this purpose were of very low
energy, it is assumed that damage was minimal. The sputter cleaning was
done to keep the surface topography of the implanted and unimplanted
specimens as similar as possible.

The aluminum concentration will lower the stacking fault energy of the
surface layer. The effect will be a reduction in the propensity of cross
slip. Normally, such a reduction reduces the work hardening rate at low
strains since it decreases dislocation multiplication and dislocation-
dislocation interactions. However, for a monotonic test on implanted
samples the effect will be small and only noticeable at very small strains
since here the plastic strain in the surface grains make up a significant
portion of the total plastic strain of the sample. This explains the
difference in flow stress at small strains and the convergence of flow
stress with increasing strain as noted in Figure 1.

Since Al ions are larger than Cu ions residual compressive stresses
will be generated in the damaged layer (with the corresponding residual
tensile stresses in the interior). This compressive residual stress will
oppose any applied tensile stress. In stress controlled fatigue this
will reduce the effective tensile stress on the surface of the material and
lower the plastic strain at the surface. The reduction of SFE and

propensity of cross-slip in the surface layer of the Al implanted samples
also reduces the tendency of PSB formation, increases the reversibility of
cyclic deformation, and reduces cyclic hardening (7). The sessile vacancy
loops formed by the ion implantation (6) act as a barrier to slip and
reduce slip distances which tends to homogenize slip in the surface region.
The slip homogeneity will be further improved by the presence of
dislocations which may be able to accommodate small cyclic slip without any
generation of additional dislocations.

The implantation shows a tendency to change the surface deformation
mode from coarse slip bands to more finer planar slip. This type of
homogeneity of deformation should reduce the extent of cyclic deformation in
each slip band. Since chances of slip reversibility improve with a
decrease in cyclic plastic strain, the deformation at the surface of the
implanted material should be more reversible. Consequently the implanted
material should show less cyclic hardening than the unimplanted material,
as observed in Figure 3.

Fatigue crack initiation in polycrystalline copper has been observed
to occur along grain boundaries at high strains (8) and along PSB's at low
strains (9, 10). In either case irreversibility of deformation of the
surface region is what leads to the cracking. In our results we have seen
that at moderate strains (regime of our LCF studies) both grain boundary
and PSB cracks are present (Figure 6). However, the propensity of PSB
crack formation is reduced for the ion implanted material. This is
expected, since as discussed earlier, implantation should decrease the
propensity of PSB formation. Our results also show that LCF fatigue life
for implanted specimens is much improved. This again agrees with our
interpretation. When deformation is made both more homogeneous and more
reversible due to implantation the incompatibility of cyclic slip in
neighboring grains is reduced and grain boundary offsets are reduced or
it takes a larger number of cycles to form a grain boundary offet of the
same size.

The slope of the Coffin-Manson plot (the cyclic ductility exponent) is
larger for the implanted material. In other words the number of reversals
to failure of the implanted and unimplanted materials appears to converge
at lower strains. There are possibly two reasons for this. Firstly, the
plot is logarithmic and even though there is a large difference between
fatigue lives of the two materials at low strains the number of cycles
appear closer in logarithmic scale. Secondly, when the imposed strain is
low the deformation is more localized and this perhaps has a stronger
control over fatigue life than the surface coating.

At the life range of $\sim 10^5$ the improvement in life due to implantation
appears to be the same for both low cycle and high cycle fatigue samples.
Since the difference in cyclic flow stress of the materials is small the
slip homogeneity and reversibility effect in LCF should also be reflected
in the HCF data. When the stress is further reduced, slip becomes
completely reversible for the implanted material and a drastic improvement
in life is observed. For the implanted material a reduction of surface
deformation and an increase in deformation homogeneity and reversibility
may have produced much better fatigue behavior in this range. As mentioned
previously, the compressive residual stress on the surface of the implanted
material will oppose the applied tensile stress and reduce the plastic
stress at the surface. Consequently, the fatigue life for a given applied
stress is longer for the copper that had been implanted with aluminum ions.

First line of text for other than title **Conclusions**

1. No significant change in monotonic yield stress due to Al ion implantation on copper was measured. However, Al ion implantation results in a small decrease in monotonic hardening at low strains.

2. Al ion implanted polycrystalline copper shows significantly less fatigue hardening than unimplanted copper.

3. An improvement in low cycle and high cycle fatigue life is observed due to Al ion implantation on polycrystalline copper. The most significant improvement appears to be the higher fatigue limit for the implanted material.

References

1. E.Y. Chen and E.A. Starke, Jr., "Effects of Ion-Plating on the Low Cycle Fatigue Behavior of Copper Single Crystals", Materials Science and Engineering, 24 (1976) pp. 209-221.

2. Shirikant P. Bhat and Campbell Laird, "High Temperature Cyclic Deformation of Nickel", Fatigue of Engineering Materials and Structures, 1 (1979) pp. 59-77.

3. Edgar A. Starke, Jr. and Gerd Lütjering, "Cyclic Plastic Deformation and Microstructure", pp. 205-243 in Fatigue and Microstructure, M. Meshii, ed.; ASM, Metals Park, Ohio, 1978.

4. L.F. Coffin, "A Study of the Effects of Cyclic Thermal Stresses on a Ductile Metal", Transactions of the ASME, 76 (1954) pp. 931-950.

5. S.S. Manson, NACA, Technical Note 2933 (1954).

6. S. Spooner and K.O. Keith, "X-Ray Diffraction Characterization of Aluminum Ion Implanted Copper Crystals:, this Symposium.

7. M. Wilhelm and P. Everwin, "Cyclic Deformation Behaviour of α-Copper and Underaged Copper-Cobalt Alloy Single Crystal", paper presented at the 5th International Conference on the Strength of Metals and Alloys in Aachen, August, 1979.

8. C. Laird and D.J. Duquette, "Mechanisms of Fatigue Crack Nucleation", pp. 88-117 in Corrosion Fatigue, Chemistry Mechanisms and Microstructure, A.J. McEvily and R.W. Staehle, eds., NACE, Houston, Texas, 1972.

9. W.H. Kim and C. Laird, "Crack Nucleation and Stage I Propagation in High Strain Fatigue-I. Microscopic and Interferometric Observations", Acta Metallurgica, 26 (1978) pp. 77-787.

10. W.H. Kim and C. Laird, "Crack Nucleation and Stage I Propagation in High Stress Fatigue-II Mechanism", Acta Metallurgica, 26 (1978) pp. 789-799.